Supporting Information for

ORIGINAL ARTICLE

Dendritic nanomedicine enhances chemo-immunotherapy by disturbing metabolism of cancer-associated fibroblasts for deep penetration and activating function of immune cells

Yunkun Li[a], **Xiaoding Shen**[a], **Haitao Ding**[a], **Yuxin Zhang**[a], **Dayi Pan**[a], **Liping Su**[a], **Yahui Wu**[a], **Zaixiang Fang**[a], **Jie Zhou**[a], **Qiyong Gong**[a,b,c], **Kui Luo**[a,b,*]

[a]*Department of Radiology, Huaxi MR Research Center (HMRRC), Frontiers Science Center for Disease-Related Molecular Network, State Key Laboratory of Biotherapy, West China Hospital, Sichuan University, Chengdu 610041, China*

[b]*Functional and Molecular Imaging Key Laboratory of Sichuan Province, and Research Unit of Psychoradiology, Chinese Academy of Medical Sciences, Chengdu 610041, China*

[c]*Department of Radiology, West China Xiamen Hospital of Sichuan University, Xiamen 361021, China*

Received 25 January 2024; received in revised form 21 February 2024; accepted 28 February 2024

*Corresponding author.

E-mail address: luokui@scu.edu.cn (Kui Luo).

Running title: Dendritic nanomedicine enhanced cancer chemo-immunotherapy efficacy

1. Experimental Section

1.1. Methods

^{1}H NMR (400 MHz) and ^{13}C NMR (100 MHz) spectra (Bruker, AVANCE NEO, Germany) were recorded on a Bruker Avance II NMR spectrometer with DMSO-*d6* as solvents and tetramethylsilane was used as an internal reference. Dynamic light scattering (DLS) was performed on a Brookhaven BIC multiangle light scattering instrument (Brookhaven, USA) and each measurement was carried out in triplicates. A fluorescence spectrophotometer (Horiba, France) was used to detect the fluorescence signal of Epi. The absorbance was read using a UV-Vis spectrometer (UV-1800, Shimadzu, Japan). A transmission electron microscope (TEM, Tecnai GF20S-TWIN, FEI, USA) was used to observe the morphology and estimate the size of assemblies in a dry state. The synergy MX microplate reader (BioTek, USA) was used to assess the optical density (OD) value for CCK-8 assays, enzyme-linked immunosorbent assays (ELISAs), and the bioluminescence level of ATP. *In vitro* cellular and immunohistochemical fluorescent images were obtained from stochastic optical reconstruction microscopy (TiA1-N-STORM, Nikon, Japan). Quantified cellular internalization, bone-marrow dendritic cell (BMDC) maturation, and *in vivo* immune cell infiltration were obtained from fluorescence activated cell sorting (FACS, BD Celesta, BD Bioscience, USA). *Ex vivo* fluorescence imaging of major organs and tumors from the tumor-bearing mice was conducted using an *in vivo* imaging system (IVIS Spectrum *In Vivo* Imaging System, USA). The paraffin slices were imaged with a fluorescence microscope (Zeiss, Germany).

1.2. Preparation of Epi-conjugated boronate-linked PEGylated Dendron (Epi-PD)

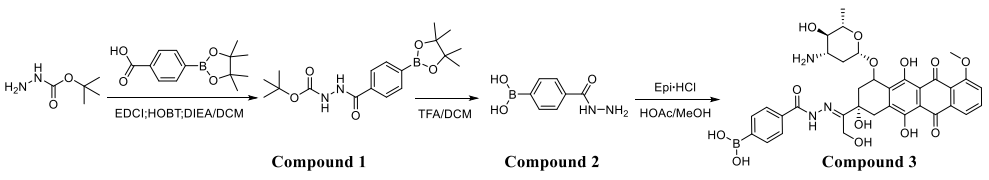

Figure S1 Synthetic process of the Epi prodrug functionalized with one PBA group.

Synthesis of Epi prodrug functionalized with one PBA group

4-Carboxybenzeneboronic acid pinacol ester (3.8 g, 15.3 mmol), *tert*-butyl carbazate

(2.0 g, 15.1 mmol), EDCI (3.5 g, 18.3 mmol) and HOBT (2.5 g, 18.5 mmol) were dissolved in anhydrous DCM under a nitrogen atmosphere. DIEA (10.0 mL, 60.4 mmol) was added slowly into the above mixture. The obtained mixture was stirred for 30 min in an ice bath and reacted for 24 h at room temperature. Thin layer chromatography (TLC) was used to monitor the reaction process. The mixture was washed sequentially with NaCl (aq), HCl (1 mol/L), and $NaHCO_3$ (aq) 3 times. The organic phase was collected and dried with Na_2SO_4. The crude product was obtained after rotary evaporation and it was then purified by column chromatography (DCM:MeOH = 10:1, *v/v*) to give **Compound 1** as a white solid (yield: 78.2%). **Compound 1** (1.0 g, 2.8 mmol) was dissolved in 4 mL DCM under a nitrogen atmosphere and TFA (4.1 mL, 55.0 mmol) was then added. The mixture reacted for 12 h to remove the Boc and pinacol groups. After removing the solvent and precipitating in diethyl ether (EE), **Compound 2** was obtained for further use.

Compound 2 (100.0 mg, 555.3 μmol) and Epi·HCl (386.5 mg, 666.4 μmol) were dissolved in MeOH with a catalytic amount of acetic acid and the mixture reacted for 24 h at room temperature. **Compound 3** was obtained as red powder after dialysis and lyophilization.

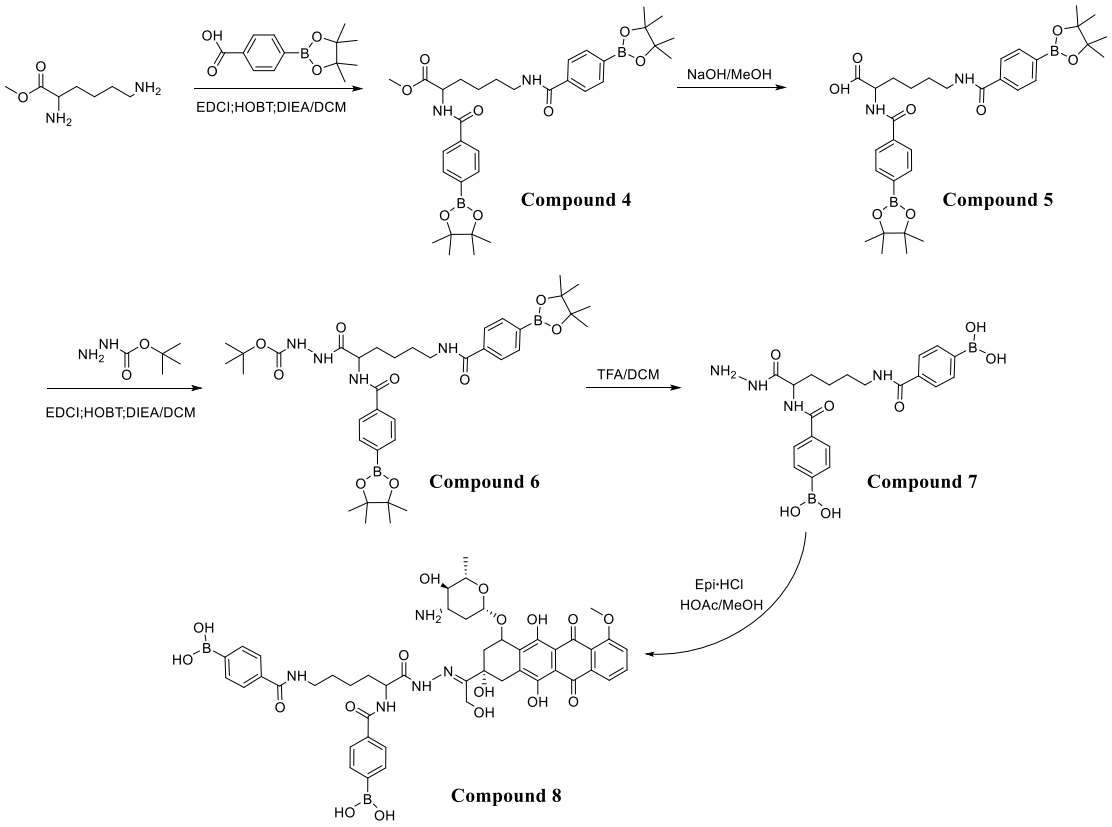

Figure S2 Synthetic process for the Epi prodrug functionalized with two PBA groups.

Functionalization of lysine

H-Lys-OMe·2HCl (2.0 g, 8.6 mmol), 4-carboxybenzeneboronic acid pinacol ester (6.4 g, 25.8 mmol), EDCI (4.9 g, 25.6 mmol), and HOBT (3.5 g, 25.9 mmol) were dissolved in anhydrous DCM under a nitrogen atmosphere. After the slow addition of DIEA (11.4 mL, 68.8 mmol), the mixture was stirred for 30 min in an ice bath and reacted for 24 h at room temperature. TLC was used to monitor the reaction process. The mixture was washed sequentially with NaCl (aq), HCl (1 mol/L), and $NaHCO_3$ (aq) 3 times. The organic phase was collected and dried with Na_2SO_4. The crude product was obtained after rotary evaporation and it was purified by column chromatography (DCM:MeOH = 10:1, *v/v*) to give **Compound 4** as a white solid (yield: 66.0%). **Compound 4** (3.0 g, 4.8 mmol) was dissolved in NaOH/MeOH (1 mol/L, 47.5 mL) and the solution was stirred at room temperature for 4 h. TLC was used to monitor the reaction process to deprotect the methoxy group. MeOH was removed in vacuo and DCM was added to dissolve the residue. HCl (1 mol/L) was added dropwise to adjust the pH to 3. The organic phase was collected and dried with

Na_2SO_4 to obtain **Compound 5** as a white solid (yield: 86.2%).

Compound 5 (2.0 g, 3.3 mmol), *tert*-butyl carbazate (0.7 g, 5.3 mmol), EDCI (1.0 g, 5.2 mmol), and HOBT (0.7 g, 5.2 mmol) were dissolved in anhydrous DCM under a nitrogen atmosphere. After the slow addition of DIEA (2.2 mL, 13.3 mmol), the mixture was stirred for 30 min in an ice bath and reacted for 36 h at room temperature. TLC was used to monitor the reaction process. The mixture was washed sequentially with NaCl (aq), HCl (1 mol/L), and $NaHCO_3$ (aq) 3 times. The organic phase was collected and dried with Na_2SO_4. The crude product was obtained after rotary evaporation and it was purified by column chromatography (DCM:MeOH = 15:1, *v/v*) to produce **Compound 6** as a white solid (yield: 80.2%). **Compound 6** (1.5 g, 2.1 mmol) was dissolved in 4 mL DCM under a nitrogen atmosphere. After the addition of TFA (4.7 mL, 62.4 mmol), the mixture reacted for 12 h to remove the Boc and pinacol groups. After removing the solvent, the residue was washed with EE to yield **Compound 7** for further use.

Synthesis of the Epi prodrug functionalized with two PBA groups

Compound 7 (200.0 mg, 438.0 μmol) and Epi·HCl (305.1 mg, 526.0 μmol) were dissolved in MeOH with a catalytic amount of acetic acid and the mixture reacted for 24 h at room temperature. The solvent was removed in vacuo. Unreacted Epi·HCl was removed by dialysis in a dialysis tube (Spectra/Por, MWCO = 1000) against deionized water for 48 h. **Compound 8** as red powder was obtained after lyophilization.

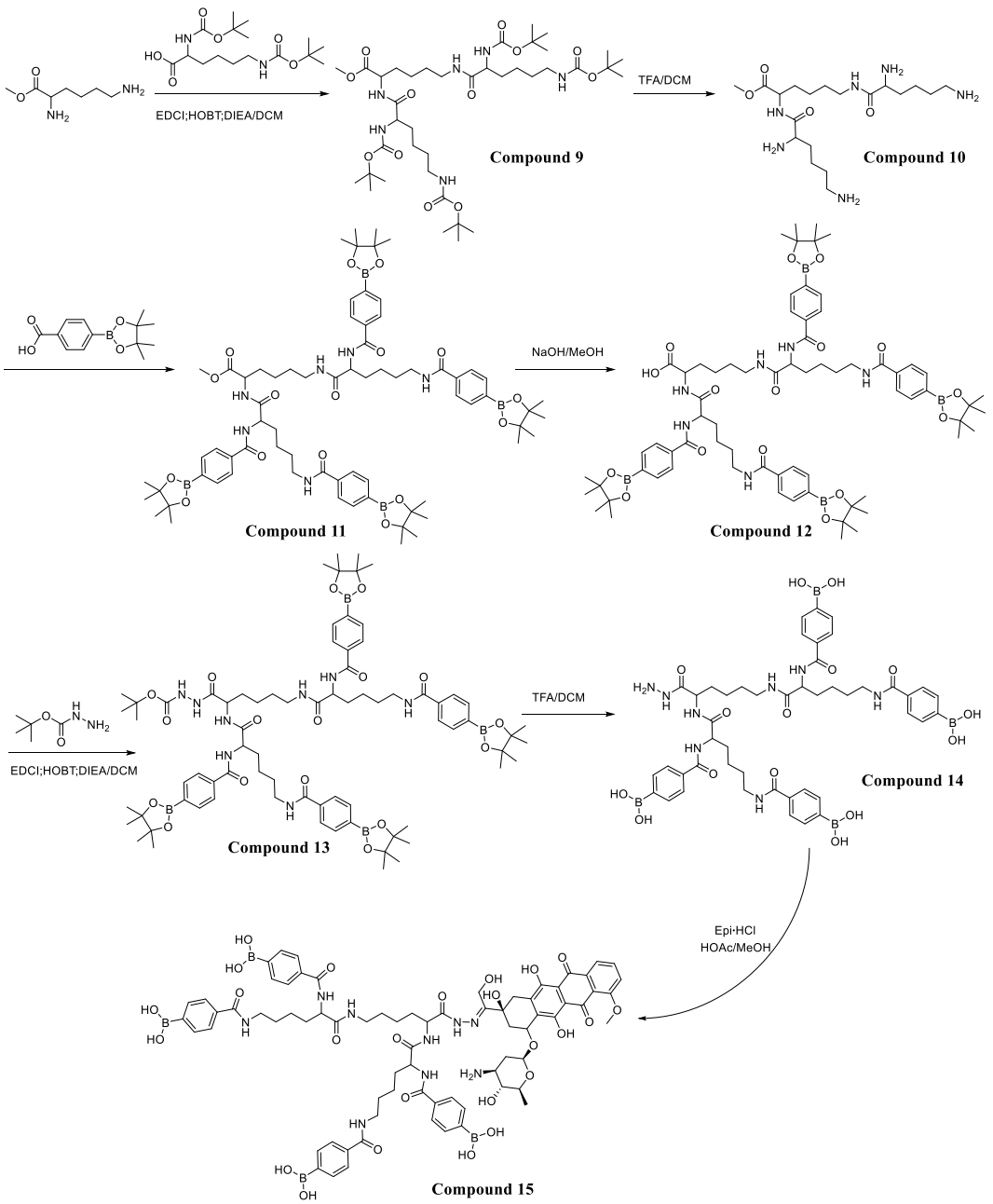

Figure S3 Synthetic process of the Epi prodrug functionalized with four PBA groups.

The step-by-step synthetic process of the Epi prodrug functionalized with four PBA groups was shown in Figure S3 and this prodrug was synthesized as previously described[1-2].

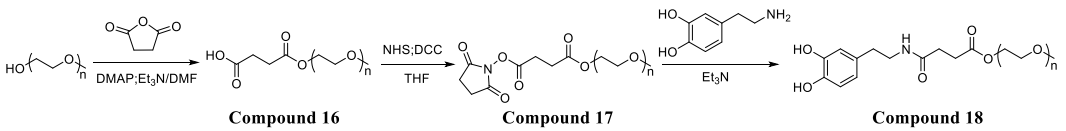

Figure S4 Synthetic process of dopamine-modified mPEG.

Synthesis of dopamine-modified mPEG

The step-by-step synthetic process of dopamine-modified mPEG was shown in Figure S4 and this prodrug was synthesized as previously described[3-4].

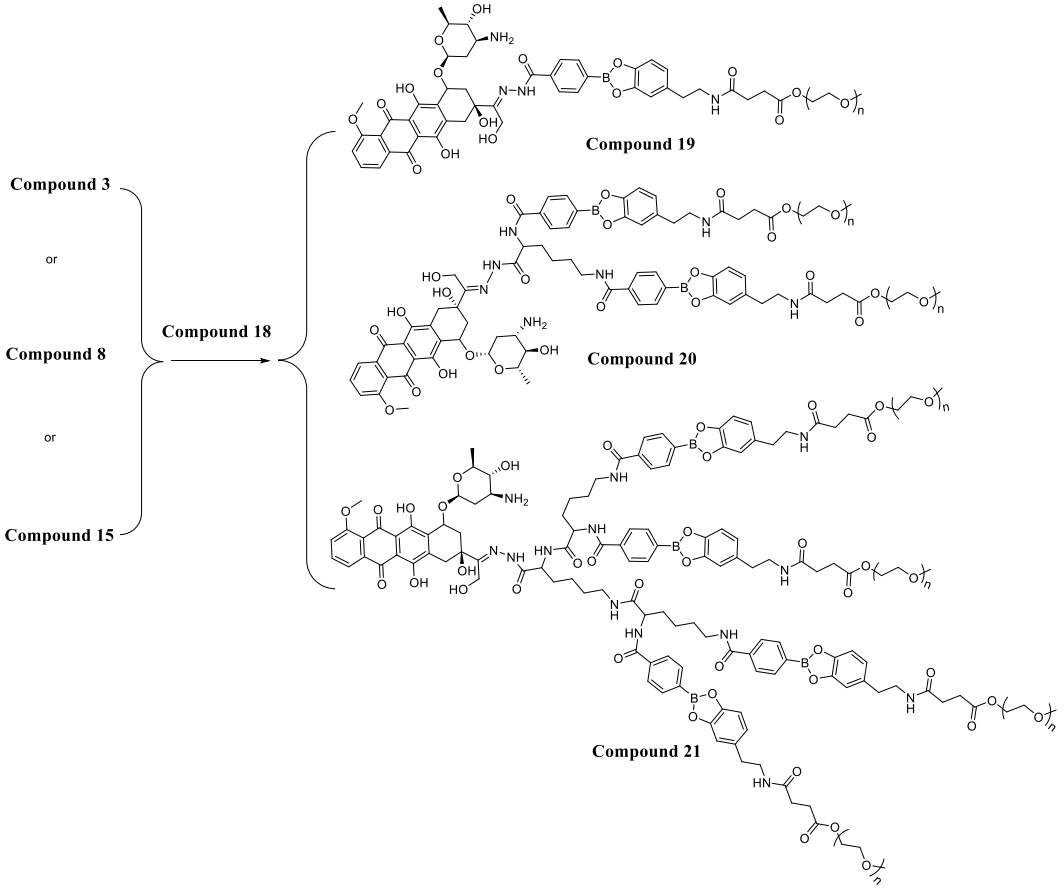

Figure S5 PEGylation of the prodrugs.

PEGylation of the Epi prodrugs

PEGylation of the prodrugs was a procedure from a boronated linker between three prodrugs and dopamine-functionalized PEG. Briefly, **Compound 3** (100.0 mg, 14.2 μmol) and **Compound 18** (210.8 mg, 17.1 μmol) were dissolved in deionized water respectively. The aqueous solution of **Compound 18** was added dropwise to the aqueous solution of **Compound 3** under stirring. After the mixture reacted in the dark for 24 h, it was transferred into a dialysis tube (Spectra/Por, MWCO = 1000) and dialyzed for 48 h against deionized water. **Compound 19** was obtained as red powder after lyophilization. **Compound 20** and **Compound 21** were obtained similarly from **Compound 8/ Compound 18** and **Compound 15/ Compound 18,** respectively.

1.3. In vitro Epi release

The *in vitro* Epi release from Epi-PD was assessed in phosphate-buffered saline (PBS) at pH 7.4, 6.5, and 5.0 at 37 °C. Epi-PD dissolved in 0.5 mL PBS was transferred into dialysis tubes (MWCO 1000) and immersed into 10 mL of the buffer solution at different pH values. 0.4 mL of the dialysate was withdrawn and an equal volume of the fresh corresponding buffer solution was replenished to maintain a constant volume. The concentration of Epi (n = 3) was obtained by measuring the fluorescence intensity at 600 nm *via* a microplate reader excited at 480 nm *via* a standard curve.

1.4. Pharmacokinetics analysis

Male BALB/c mice (n = 4) were randomly divided into 4 groups and they were intravenously administrated with Epi·HCl, Epi-P1D, Epi-P2D, or Epi-P4D at an Epi dosage of 5 mg/kg. Blood samples were collected from the orbital venous plexus at 0.25, 0.5, 1, 3, 6, 9, 12, 24, and 48 h post-injection and centrifuged at 5000 rpm for 5 min. The supernatant was collected and treated with 5 mol/L HCl at 50 °C for 90 min. When cooling to room temperature, 1 mol/L sodium hydroxide was added. After chloroform/isopropanol (*v/v*, 4:1) was added, the mixture was vortexed for 90 s. The organic phase was collected after centrifugation at 10000 g for 5 min and dried at room temperature overnight. 100 μL of DMSO was added to dissolve Epi and the absorbance of the sample was read by a microplate reader.

1.5. Cytokine secretion in blood serum and tumor tissue

On Day 2 after the last intravenous administration of saline, Epi·HCl, Epi-P1D, Epi-P2D, or Epi-P4D every three days 4 times at an Epi dosage of 5 mg/kg, the blood and tumors were harvested to measure the levels of cytokines, including granzyme B, perforin, tumor necrosis factor α (TNF-α) and interferon γ (IFN-γ). The serum was obtained after centrifugation at 2000 rpm for 5 min. The tumor tissues were homogenized in PBS containing 1 mmol/L PMSF and the supernatant was collected. The cytokines in the serum and tumor tissues were detected with ELISA kits according to the manufacturer's instructions.

2. Supplementary figures

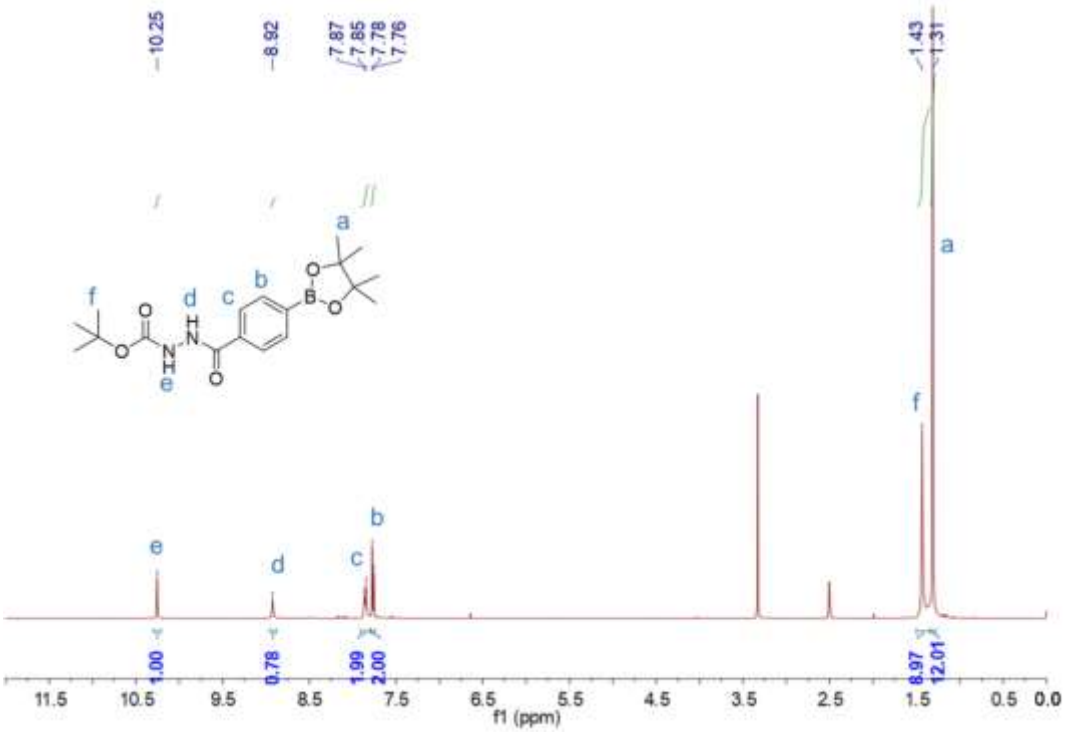

Figure S6 ^{1}H NMR spectrum of **Compound 1** in DMSO-*d6*.

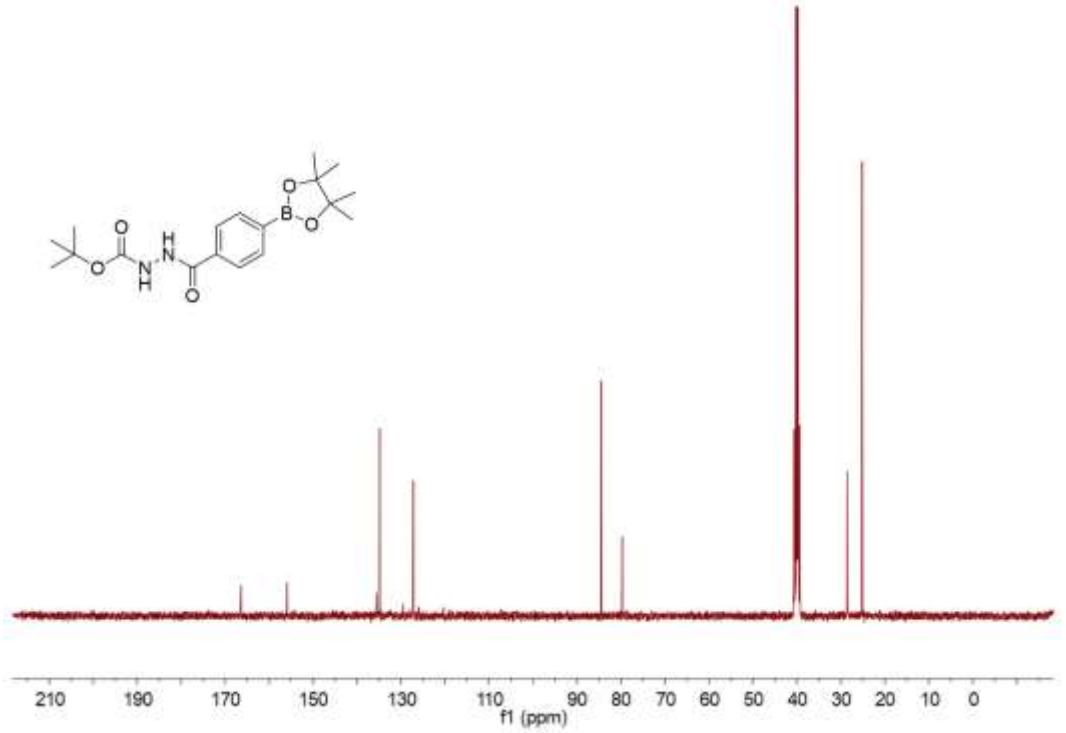

Figure S7 ^{13}C NMR spectrum of **Compound 1** in DMSO-*d6*.

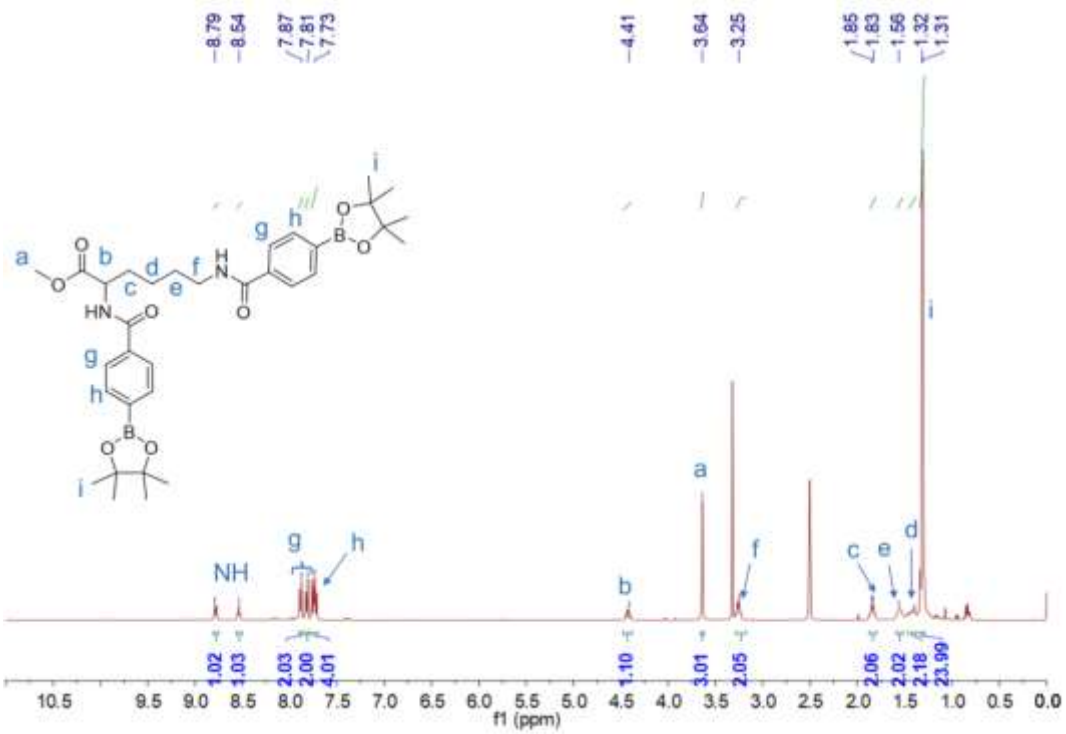

Figure S8 ^{1}H NMR spectrum of **Compound 4** in DMSO-*d6*.

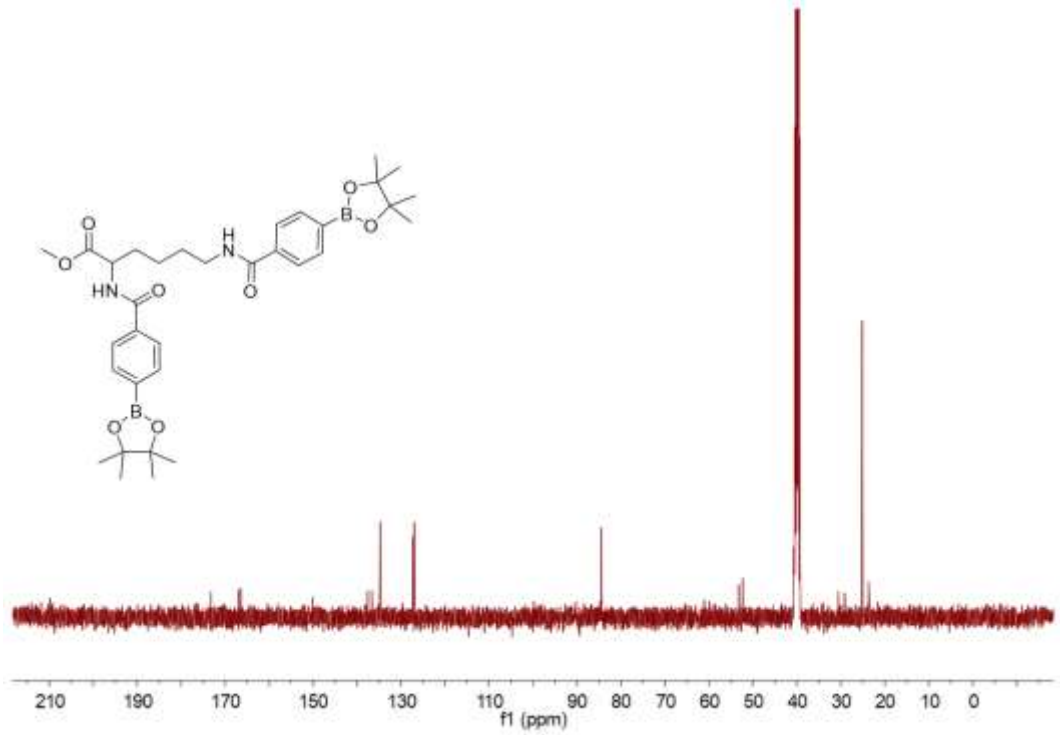

Figure S9 ^{13}C NMR spectrum of **Compound 4** in DMSO-*d6*.

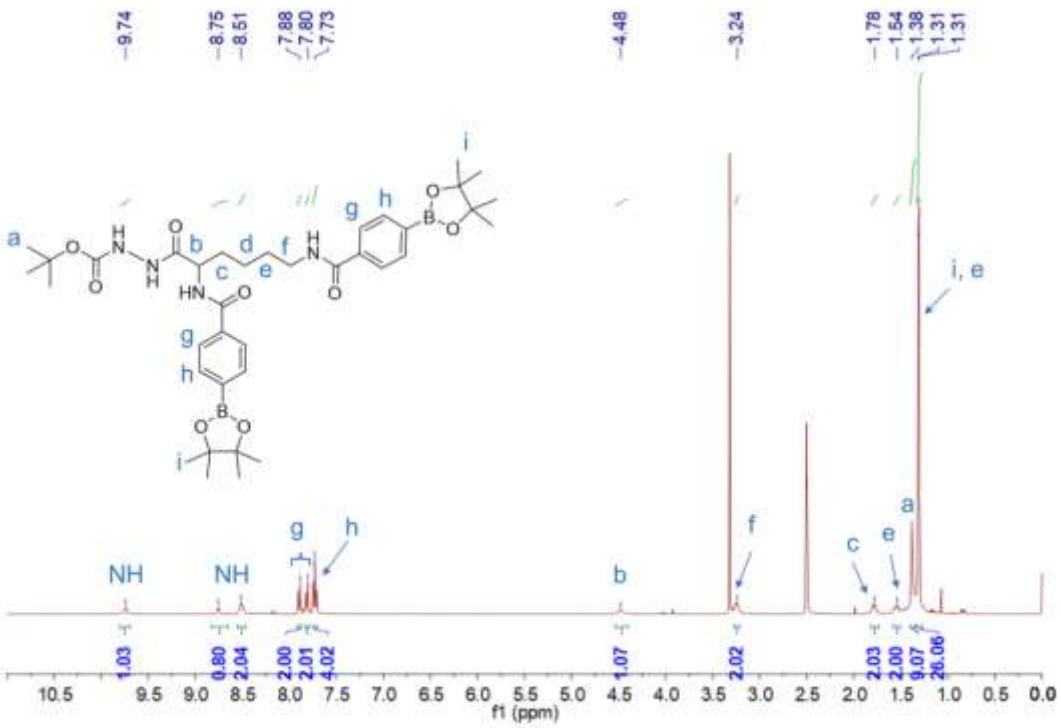

Figure S10 ^{1}H NMR spectrum of **Compound 6** in DMSO-*d6*.

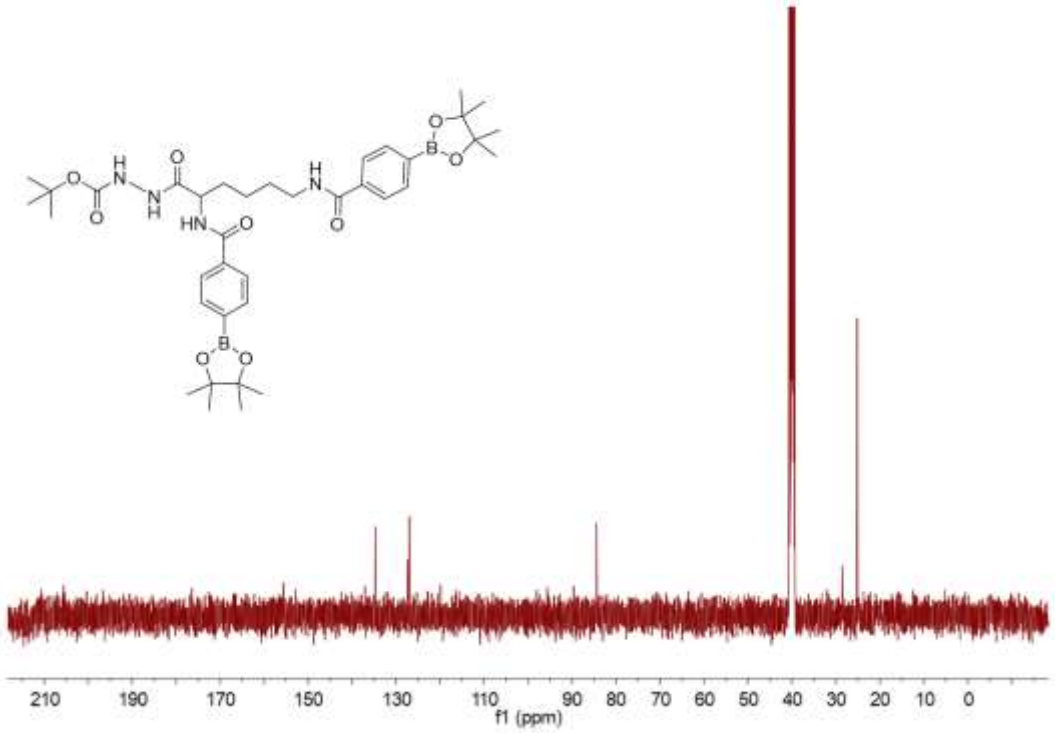

Figure S11 ^{13}C NMR spectrum of **Compound 6** in DMSO-*d6*.

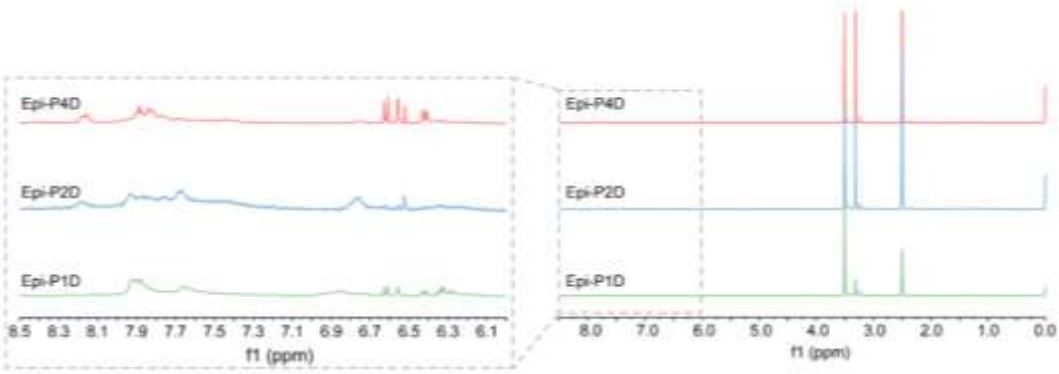

Figure S12 ^{1}H NMR spectra (right) of Epi-P1D, Epi-P2D, and Epi-P4D in DMSO-*d6* and an enlarged view of their ^{1}H NMR spectra between 8.5-6.0 ppm (left).

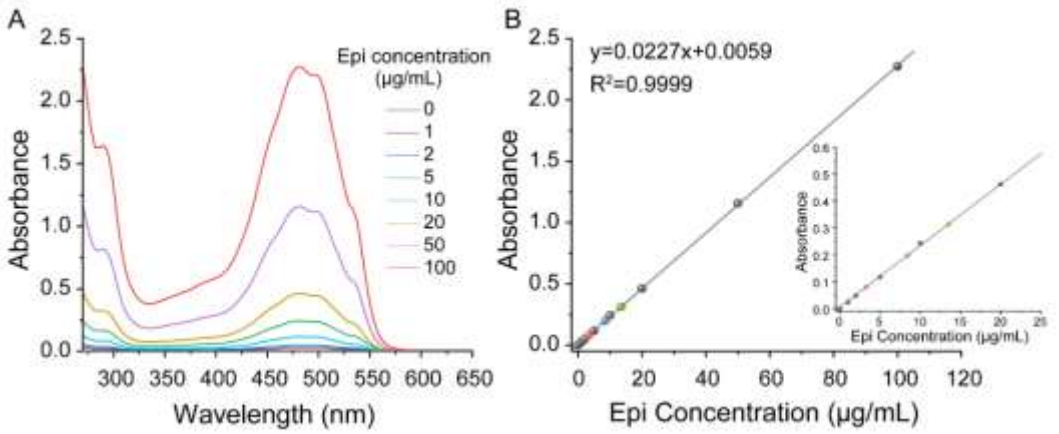

Figure S13 (A) UV–vis spectra of Epi·HCl in DMSO at various Epi concentrations ranging from 1 μg/mL to 100 μg/mL. (B) The linear fitting curve for the Epi absorbance at 480 nm as a function of the Epi concentration and an enlarged view of the curve at an Epi concentration of 0–25 μg/mL (inset). Green, blue, and red dots represent the absorbance of Epi-P1D, Epi-P2D, and Epi-P4D at an Epi concentration of 50 μg/mL, respectively.

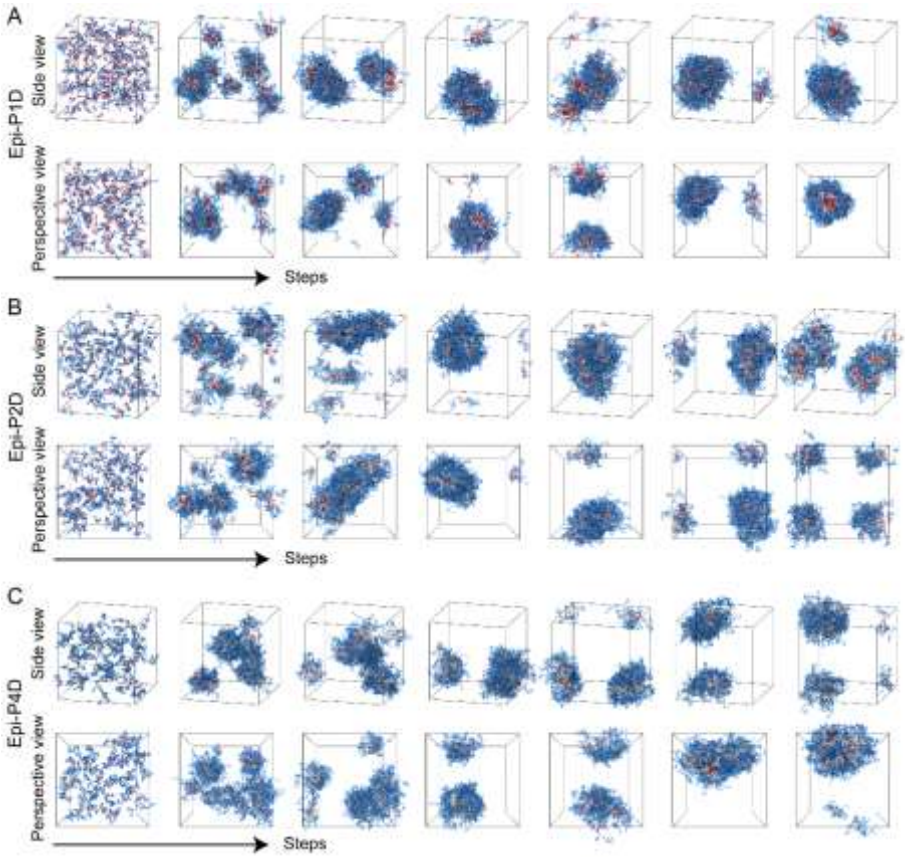

Figure S14 Simulation of the self-assembly process of (A) Epi-P1D, (B) Epi-P2D, and (C) Epi-P4D in a side view and a perspective view.

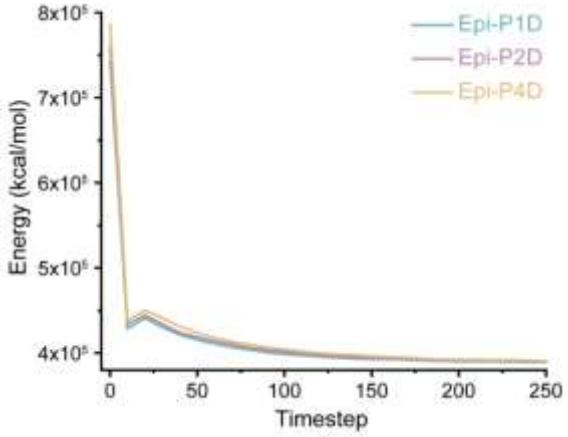

Figure S15 Temporal evolution of the total potential energy during the self-assembly process of Epi-P1D, Epi-P2D, and Epi-P4D. The total potential energy generally decreased during the self-assembly process. The diagram suggested that Epi-PD reached a steady state at around 150 timestep. There was no significant difference in the total potential energy during the self-assembly process among Epi-P1D, Epi-P2D, and Epi-P4D.

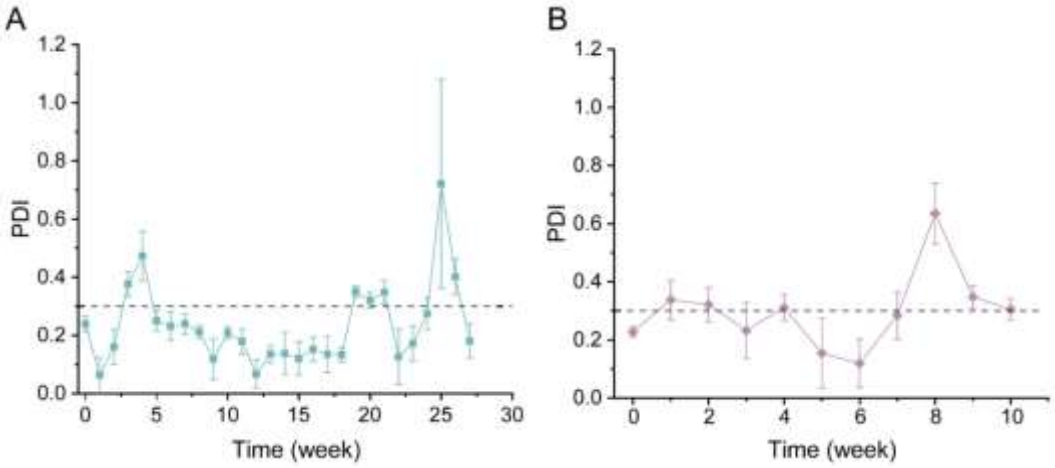

Figure S16 PDI variations of (A) Epi-P1D and (B) Epi-P2D in H_2O.

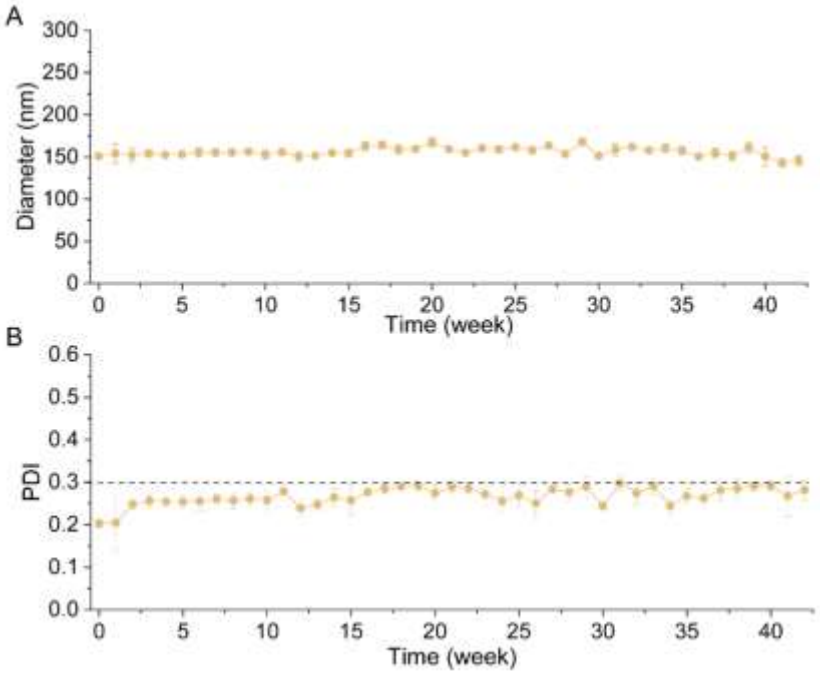

Figure S17 (A) Size variations and (B) PDI variations of Epi-P4D in H_2O.

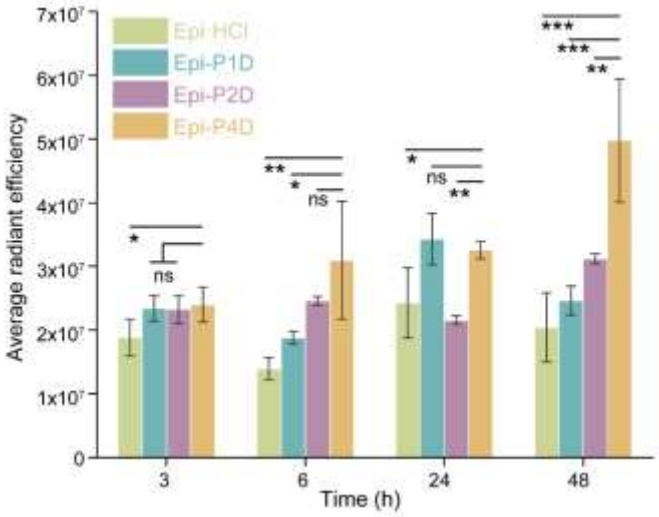

Figure S18 Average radiant efficiencies in the *ex vivo* images of major organs and tumors of the CT26 tumor-bearing mice (Data are mean ± SD, n = 3). ns, not significant, *P < 0.05, **P < 0.01, and ***P < 0.001 compared with the fluorescence signal of the tumor tissue harvested from the group treated with Epi-P4D.

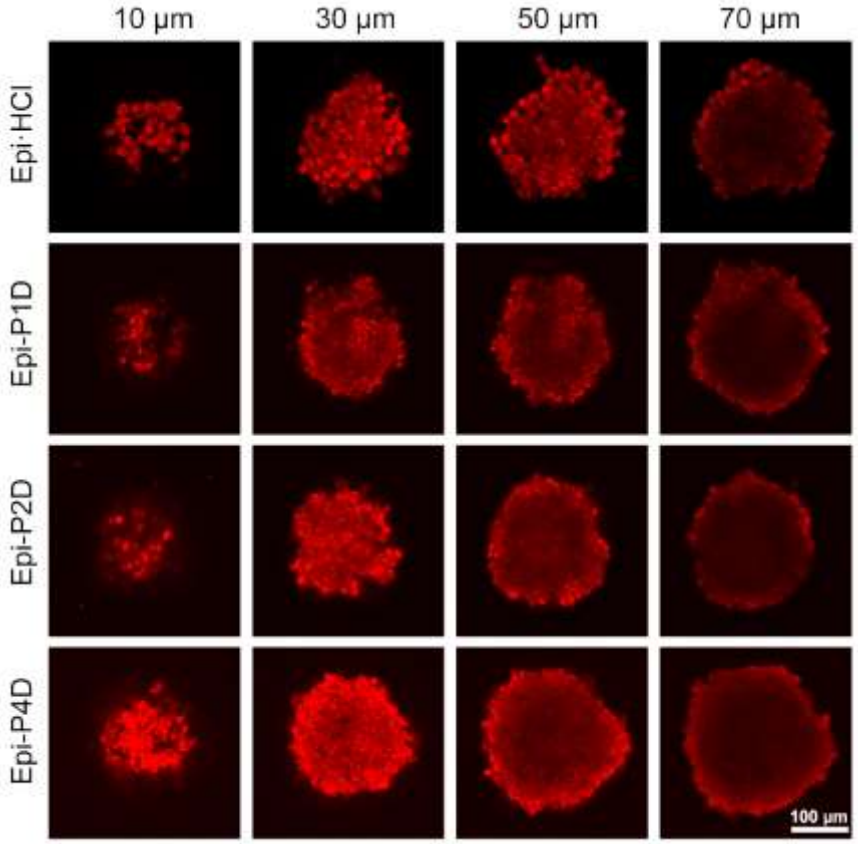

Figure S19 CLSM images of 4T1 multicellular tumor spheroids (MTSs) at different depths after incubation with Epi·HCl or Epi-PD at an equivalent Epi concentration of 10 μg/mL for 4 h.

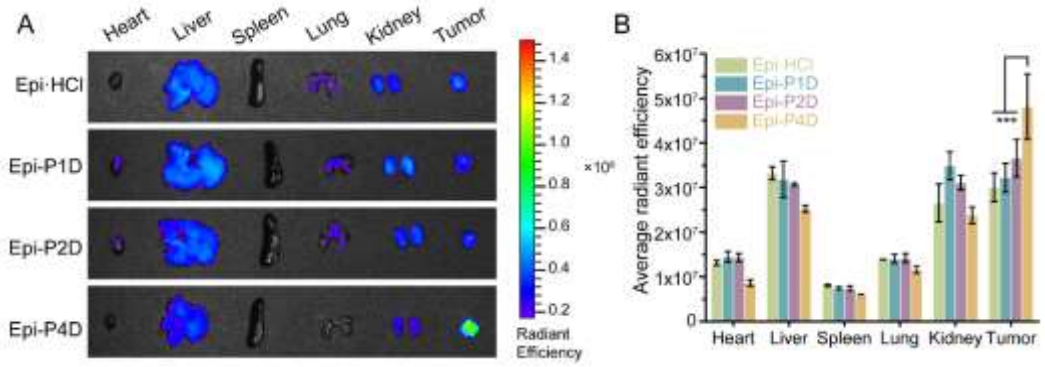

Figure S20 (A) *Ex vivo* images of major organs and tumors of the 4T1 tumor-bearing mice at 24 h post-injection of Epi·HCl, Epi-P1D, Epi-P2D, or Epi-P4D. (B) Average radiant efficiencies in the *ex vivo* images of major organs and tumors (Data are mean ± SD, $n = 3$). ***$P < 0.001$ compared with the fluorescence signal of the tumor tissue harvested from the group treated with Epi-P4D.

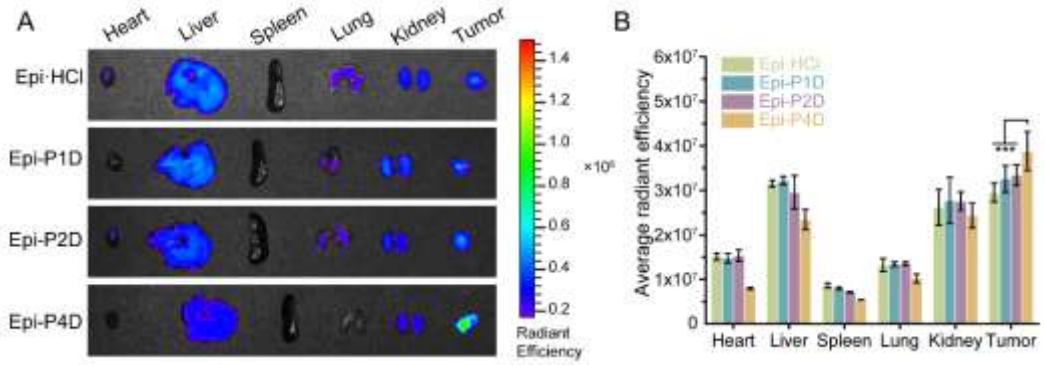

Figure S21 (A) *Ex vivo* images of major organs and tumors of the 4T1 tumor-bearing mice at 48 h post-injection of Epi·HCl, Epi-P1D, Epi-P2D, or Epi-P4D. (B) Average radiant efficiencies in the *ex vivo* images of major organs and tumors (Data are mean ± SD, $n = 3$). ***$P < 0.001$ compared with the fluorescence signal of the tumor tissue harvested from the group treated with Epi-P4D.

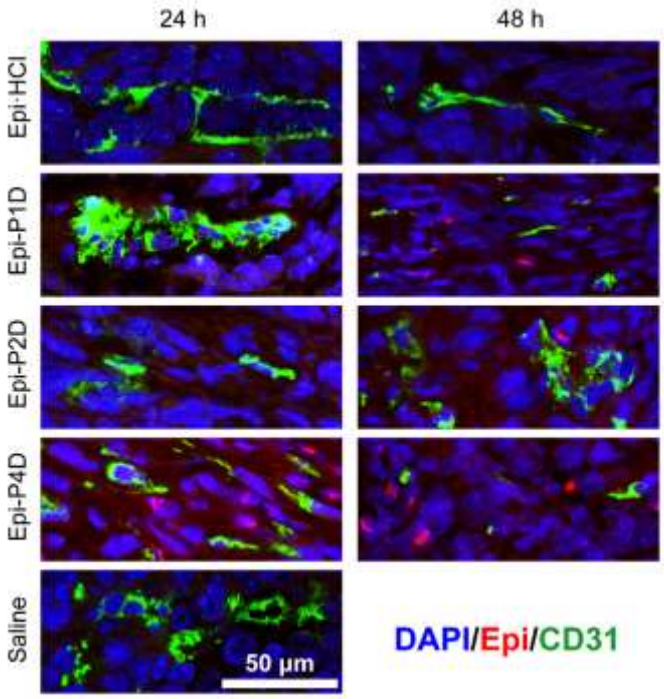

Figure S22 CLSM images of cryosections of 4T1 tumors after intravenous injection of saline, Epi·HCl, Epi-P1D, Epi-P2D, or Epi-P4D at an equivalent Epi dose of 8 mg/kg for 24 or 48 h. The tumor blood vessels were stained with CD31 (green) and the nuclei were stained with DAPI (blue). The red signal was from Epi in Epi·HCl or Epi-PD.

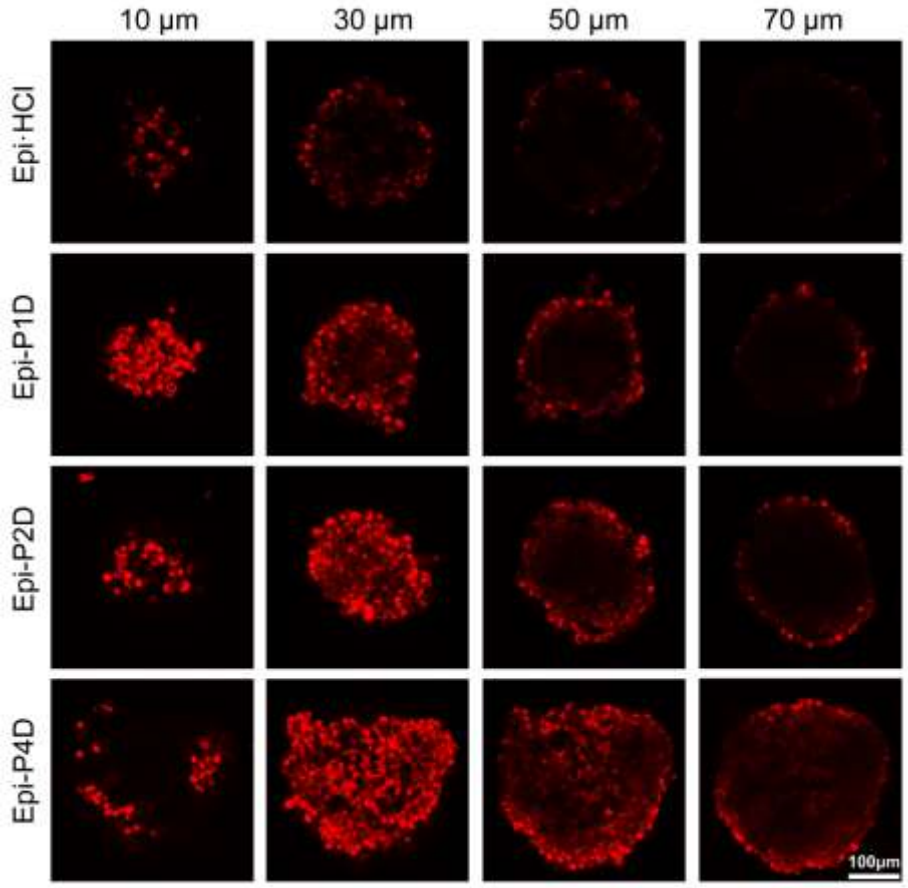

Figure S23 CLSM images of MDA-MB-231 MTSs at different depths after incubation with Epi·HCl or Epi-PD an equivalent Epi concentration of 10 μg/mL for 4 h.

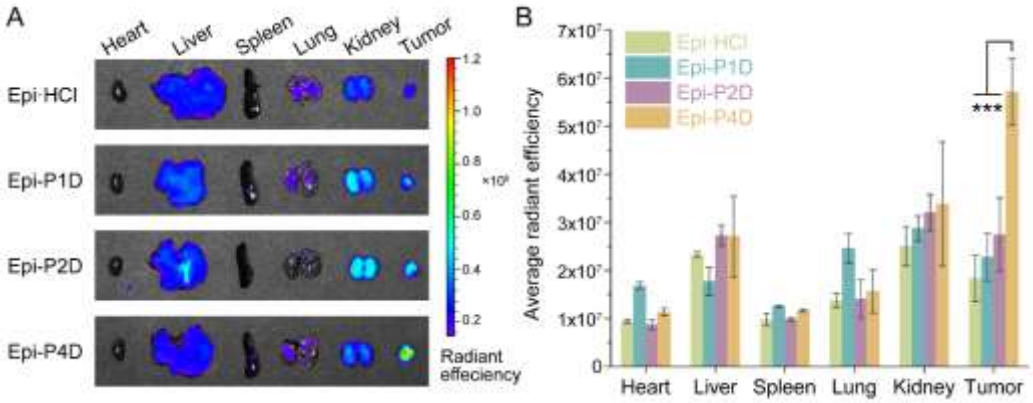

Figure S24 (A) *Ex vivo* images of major organs and tumors of the MDA-MB-231 tumor-bearing mice at 24 h post-injection of Epi·HCl, Epi-P1D, Epi-P2D, or Epi-P4D. (B) Average radiant efficiencies in the *ex vivo* images of major organs and tumors (Data are mean ± SD, $n = 3$). ***$P < 0.001$ compared with the fluorescence signal of the tumor tissue harvested from the group treated with Epi-P4D.

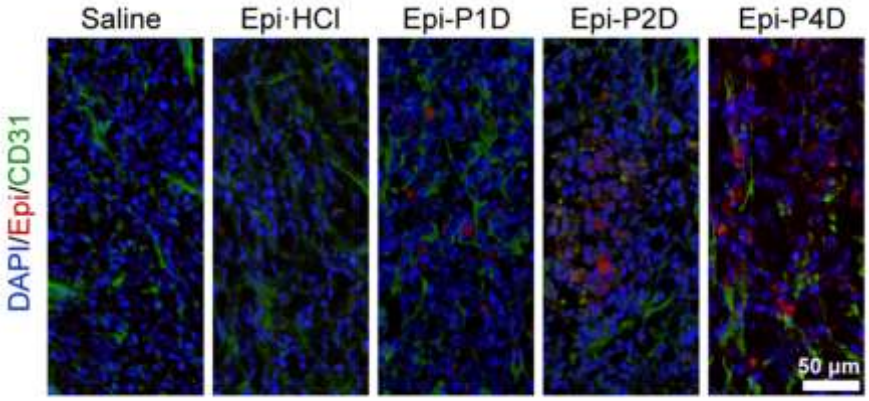

Figure S25 CLSM images of cryosections of MDA-MB-231 tumors after intravenous injection of saline, Epi·HCl, Epi-P1D, Epi-P2D, or Epi-P4D at an equivalent Epi dose of 8 mg/kg for 24 h. The tumor blood vessels were stained with CD31 (green) and the nuclei were stained with DAPI (blue). The red signal was from Epi in Epi·HCl or Epi-PD.

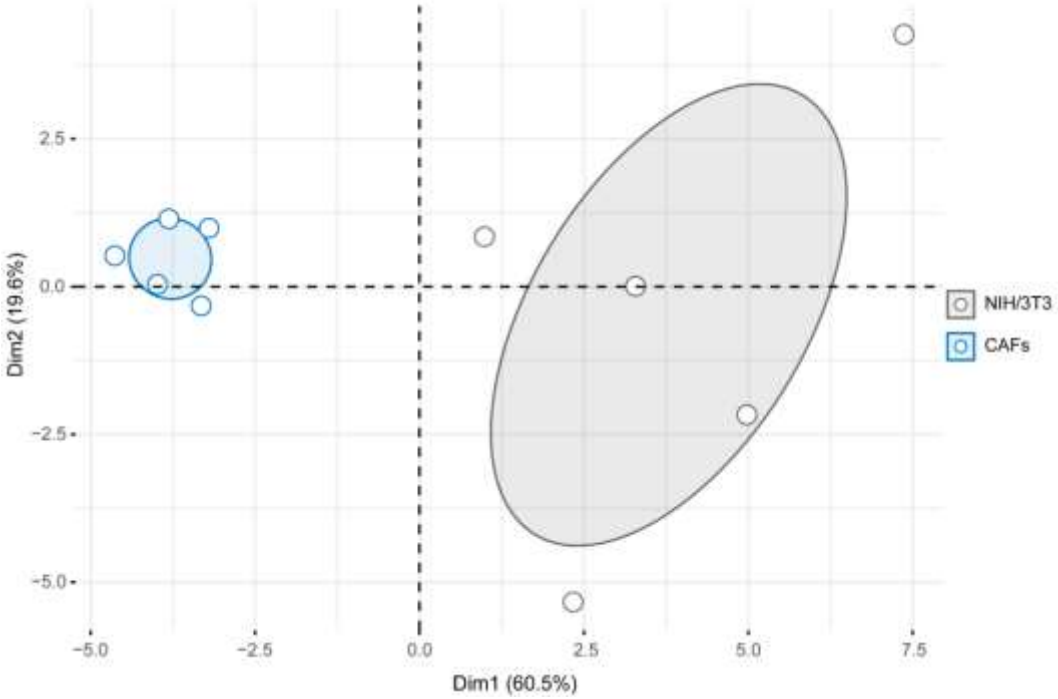

Figure S26 Principal component analysis (PCA) of the amino acid metabolism between CAFs and NIH/3T3 cells.

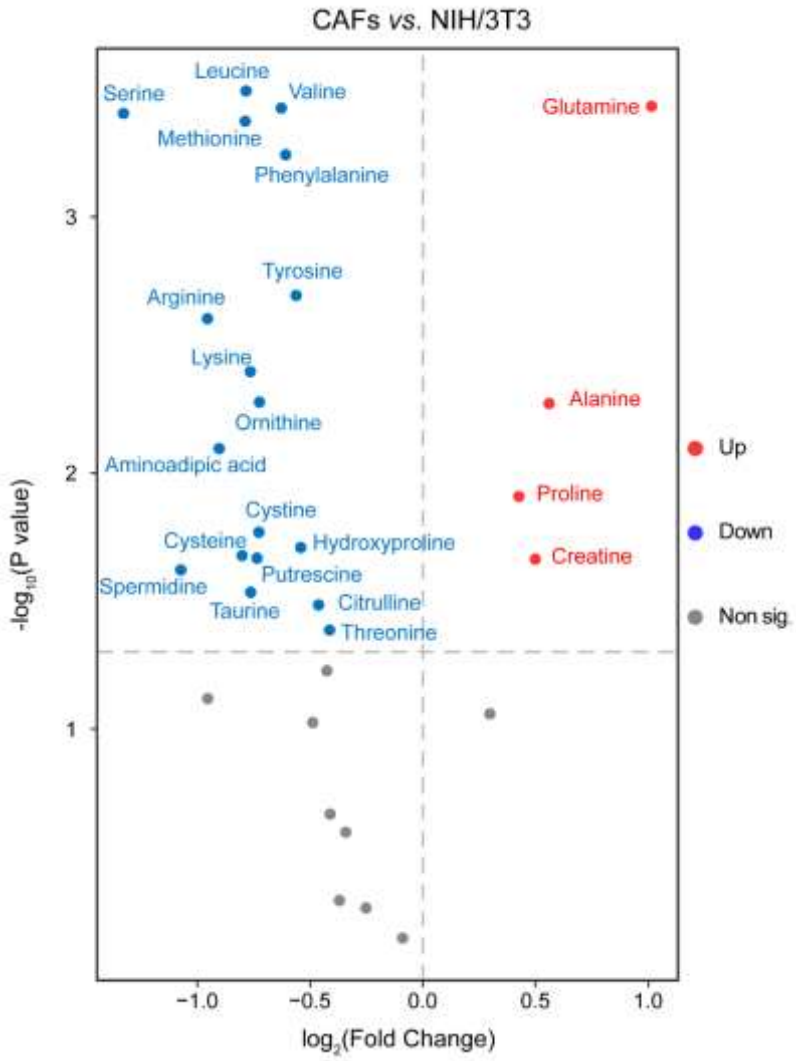

Figure S27 Volcano plot of differential amino acids between CAFs and NIH/3T3 cells.

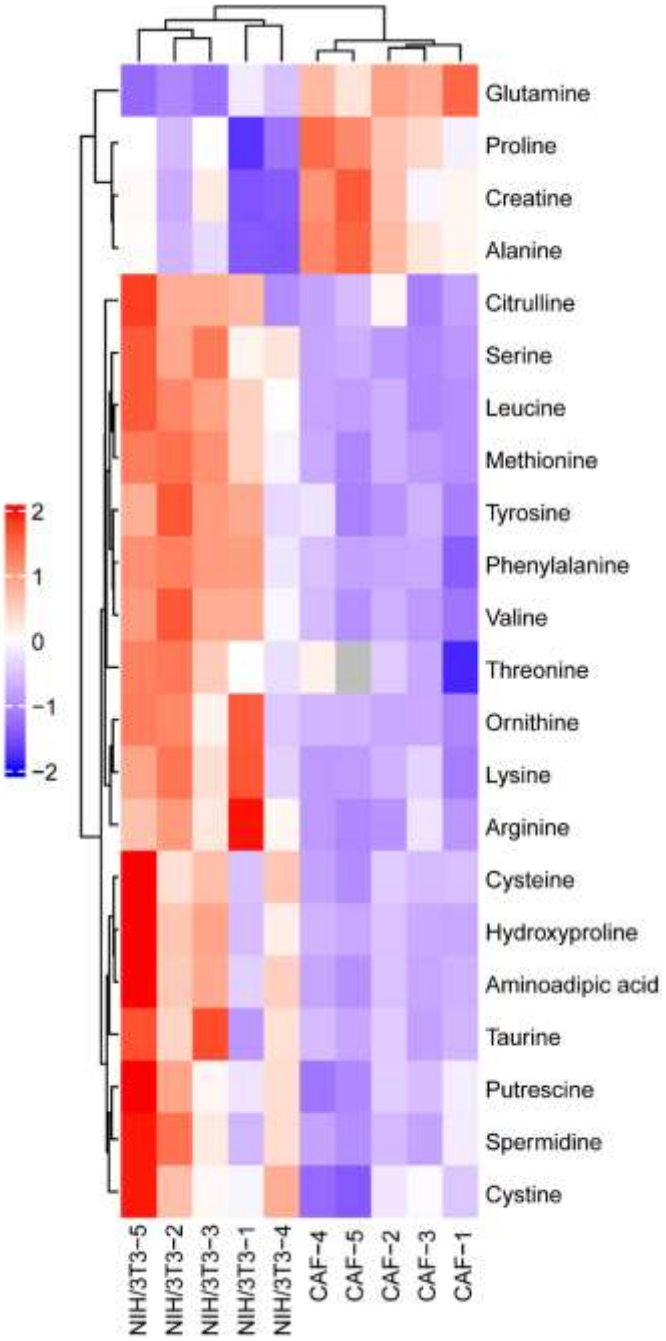

Figure S28 Heatmap of differential amino acids between NIH/3T3 cells and CAFs. NIH/3T3 1–5 and CAFs 1–5 represent five replicates of NIH/3T3 cells and CAFs without any treatment, respectively.

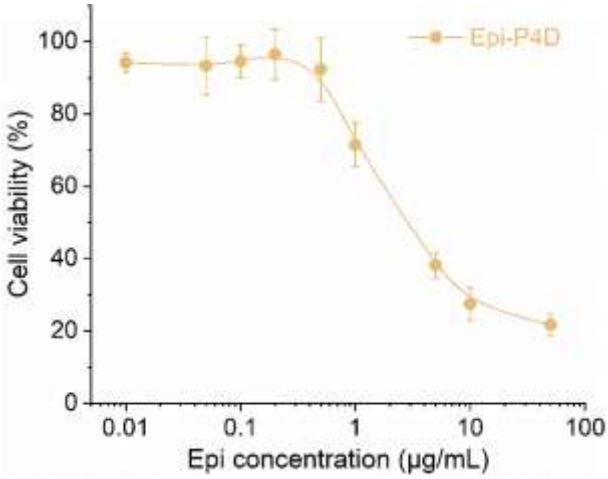

Figure S29 Cell viabilities of CAFs after incubation with Epi-P4D at various Epi concentrations for 24 h (Data are mean ± SD, n = 5).

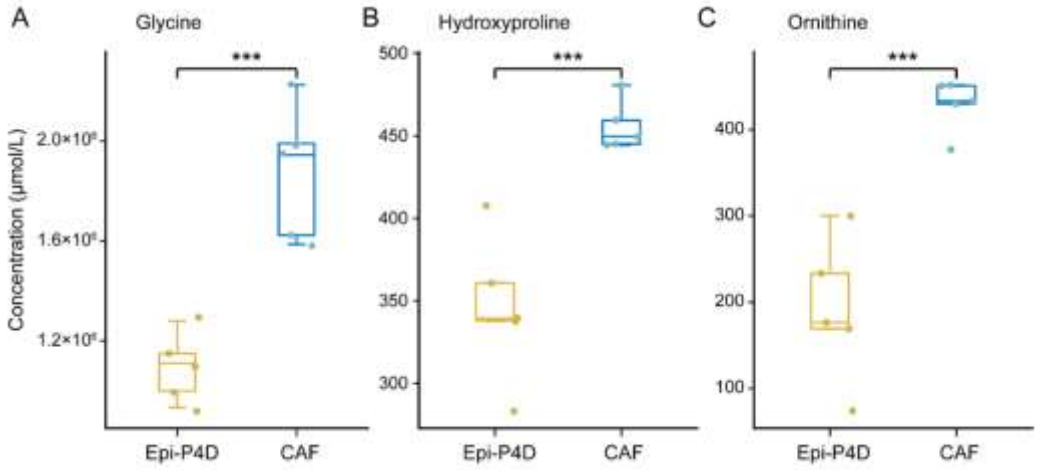

Figure S30 The concentrations of (A) glycine, (B) hydroxyproline, and (C) ornithine in the Epi-P4D-treated CAFs and CAFs without any treatment (Data are mean ± SD, n = 5). ***P < 0.001.

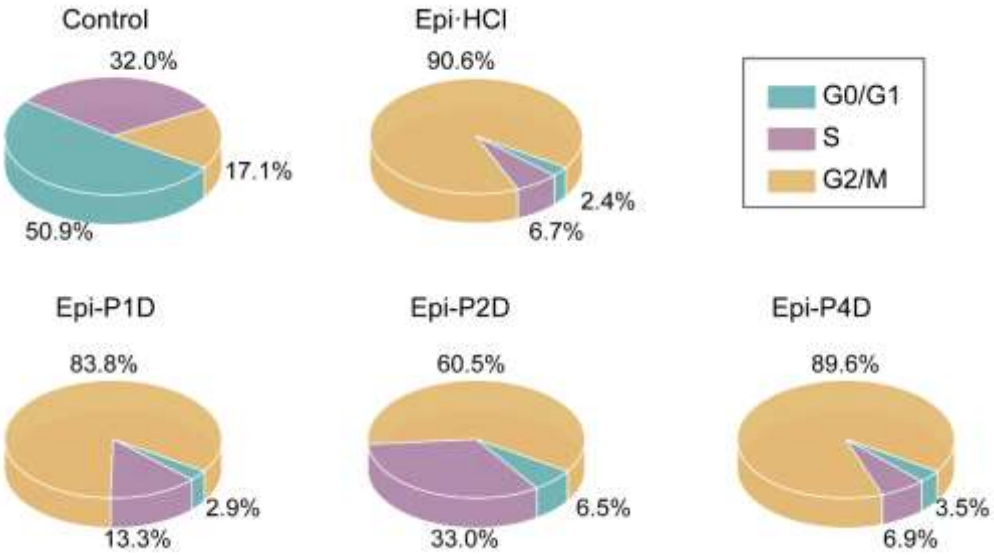

Figure S31 Cell cycle distribution of CT26 cells after treatment with Epi·HCl, Epi-P1D, Epi-P2D, or Epi-P4D at an Epi concentration of 1 μg/mL for 24 h (Data are mean ± SD, n = 3). CT26 cells without any treatment were used as a control.

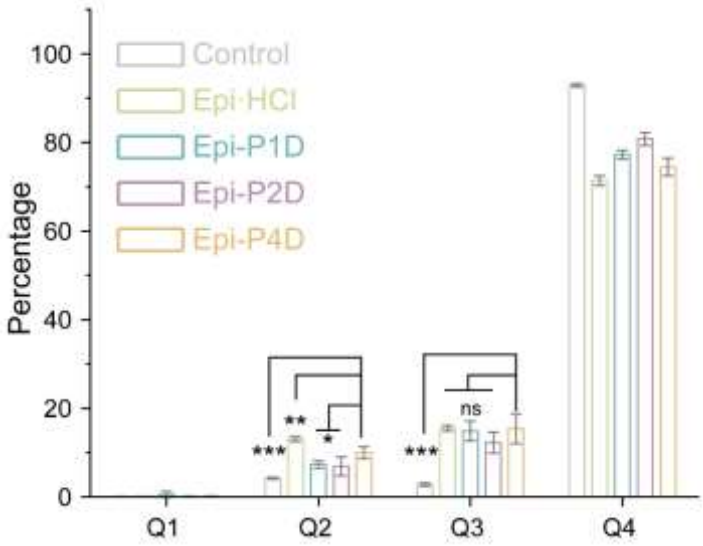

Figure S32 The percentages of apoptotic CT26 cells after treatment with Epi·HCl, Epi-P1D, Epi-P2D, or Epi-P4D at an Epi concentration of 0.3 μg/mL for 24 h (Data are mean ± SD, n = 3). CT26 cells without any treatment were used as a control. Q1, Annexin V-FITC$^-$DAPI$^+$ cells; Q2, Annexin V-FITC$^+$DAPI$^+$ cells; Q3, Annexin V-FITC$^+$DAPI$^-$ cells; Q4, Annexin V-FITC$^-$DAPI$^-$ cells. ns, not significant, *P < 0.05, **P < 0.01, and ***P < 0.001 compared with the group treated with Epi-P4D.

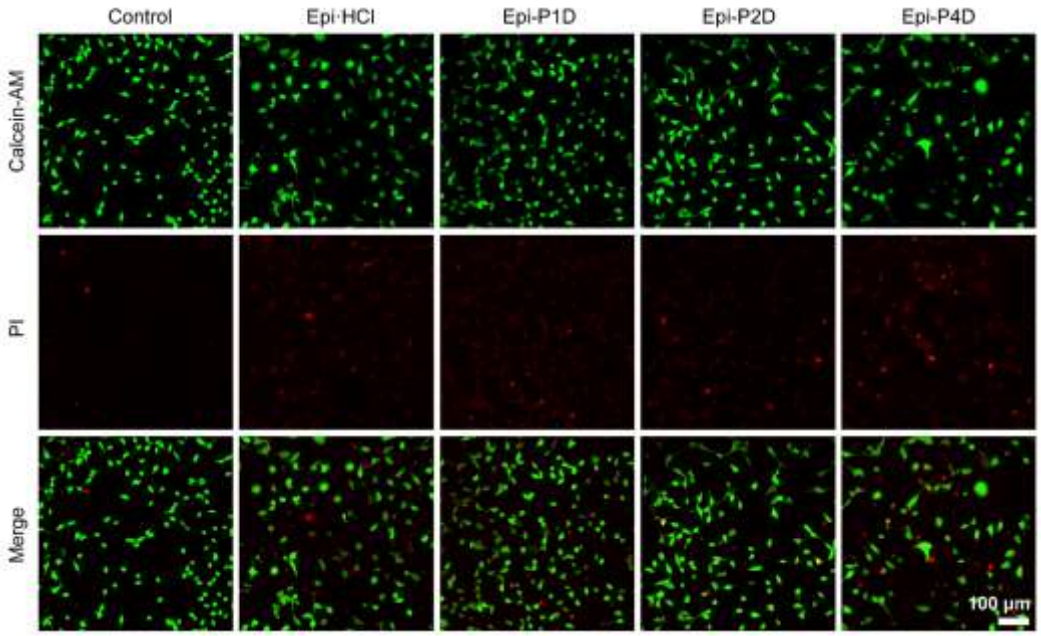

Figure S33 Calcein-AM/PI staining images of CT26 cells after treatment with Epi·HCl or Epi-PD at an Epi concentration of 0.3 μg/mL for 24 h.

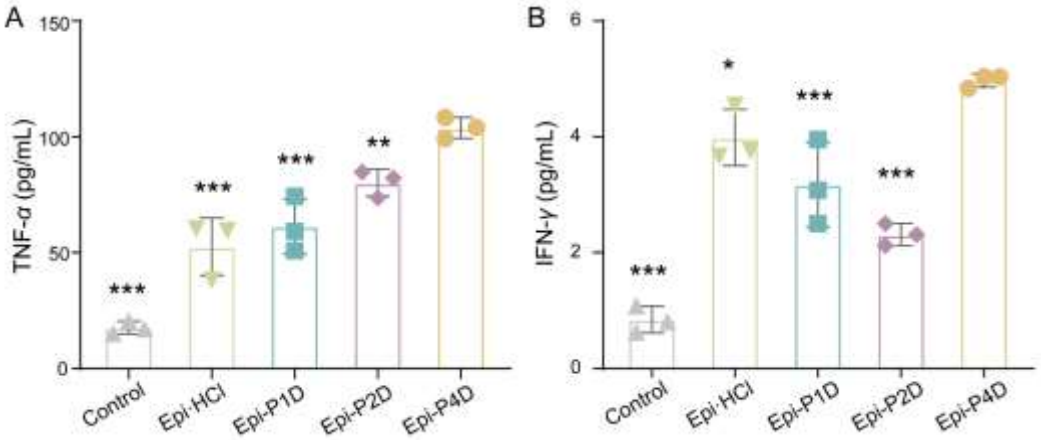

Figure S34 (A) TNF-α and (B) IFN-γ secreted by BMDCs after different treatments (Data are mean ± SD, n = 3). *P < 0.05, **P < 0.01, and ***P < 0.001 compared with the group treated with Epi-P4D.

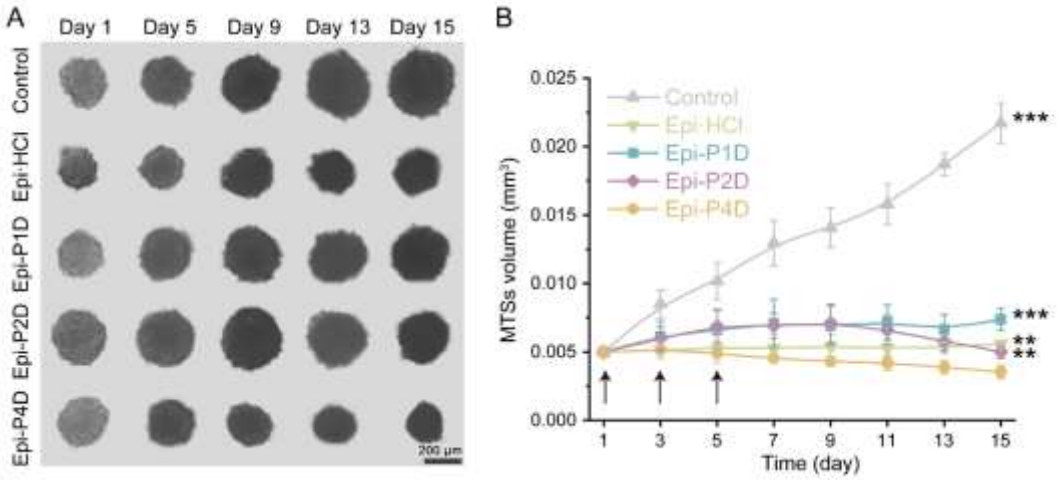

Figure S35 Photographs of CT26 MTSs on Day 1, 5, 9, 13, and 15 after treatment with Epi·HCl or Epi-PD at an Epi concentration of 1 μg/mL every other day 3 times. (B) Changes in the volume of MTSs after different treatments (Data are mean ± SD, n = 5). $^{**}P < 0.01$, and $^{***}P < 0.001$ compared with the group treated with Epi-P4D.

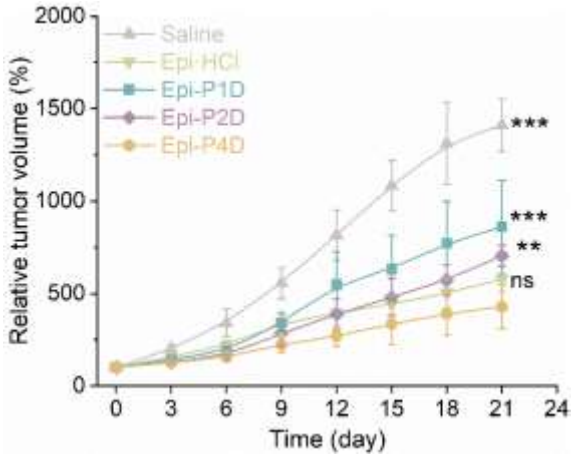

Figure S36 *In vivo* tumor growth curves of the CT26 tumor-bearing mice after treatment with saline, Epi·HCl, Epi-P1D, Epi-P2D, or Epi-P4D (an Epi dosage of 5 mg/kg, data are mean ± SD, n = 5) for 21 days. ns, not significant, $^{**}P < 0.01$, and $^{***}P < 0.001$ compared with the group treated with Epi-P4D.

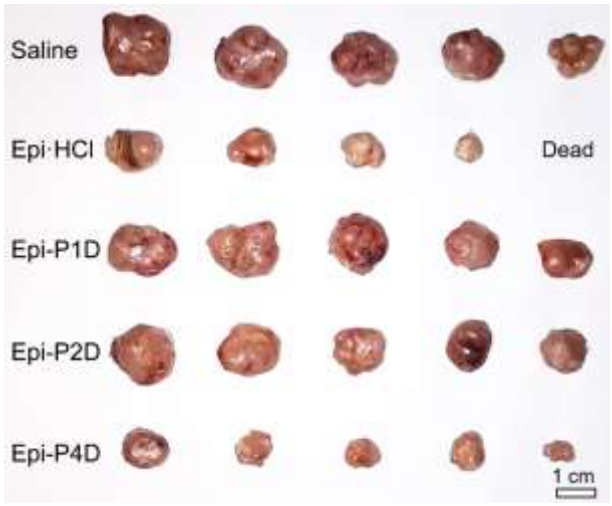

Figure S37 Images of CT26 tumors extracted from the mice on Day 21 after different treatments.

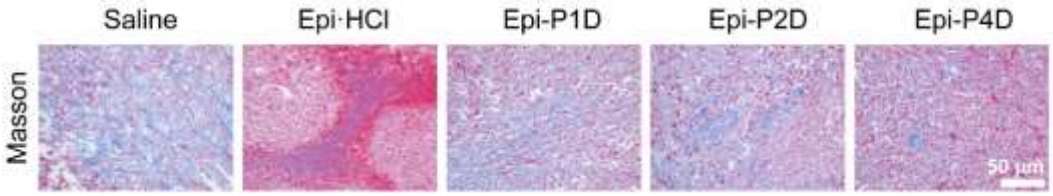

Figure S38 Immunohistochemical staining images for collagen (masson staining, blue) of the CT26 tumor tissues after treatment with Epi·HCl or Epi-PD.

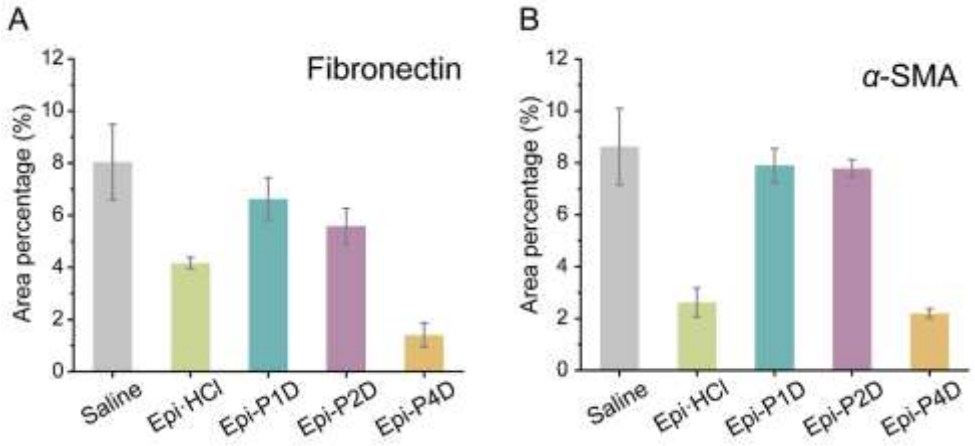

Figure S39 The levels of (A) fibronectin and (B) α-SMA in CT26 tumor tissues (Data are mean ± SD, n = 4).

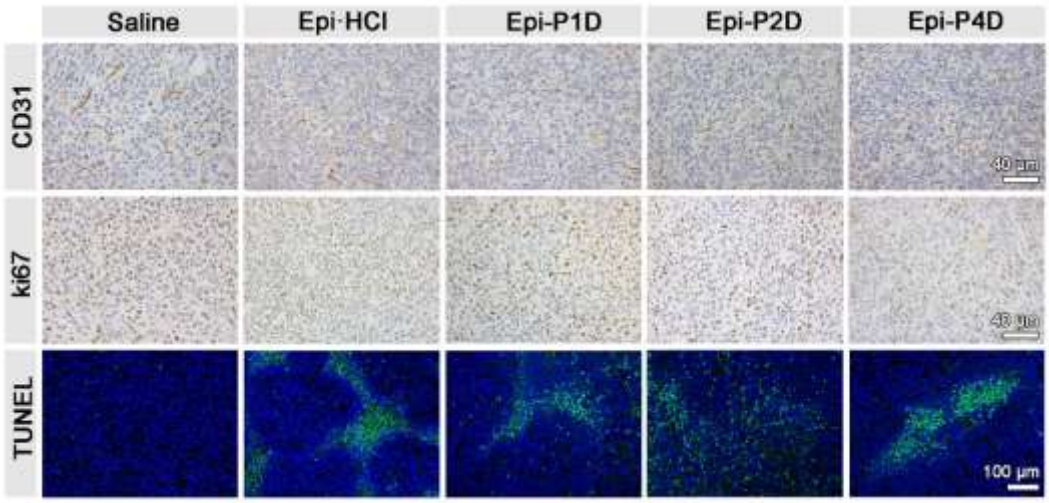

Figure S40 Immunohistochemical staining images of CD31 (brown) and ki67 (brown), and terminal-deoxynucleotidyl transferase-mediated dUTP-biotin nick end labeling (TUNEL, green) images of the CT26 tumor tissues after treatment with Epi·HCl or Epi-PD.

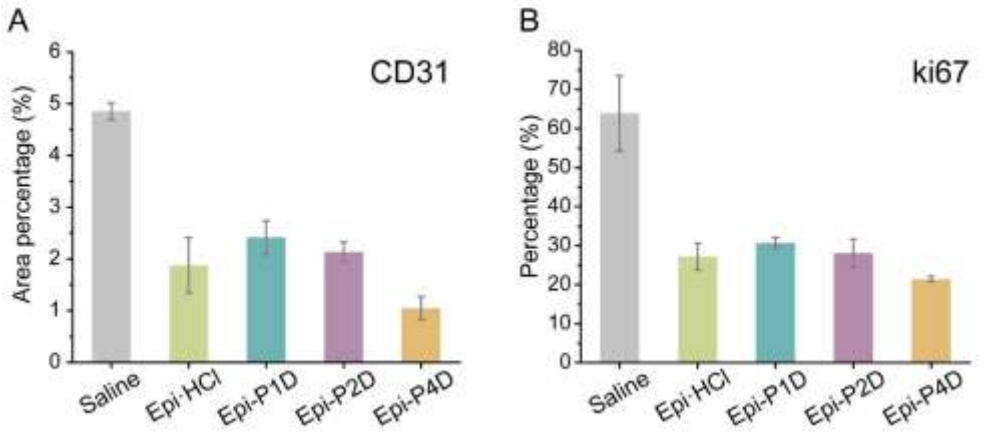

Figure S41 The levels of (A) CD31 and (B) ki67 in the CT26 tumor tissues (Data are mean ± SD, n = 4).

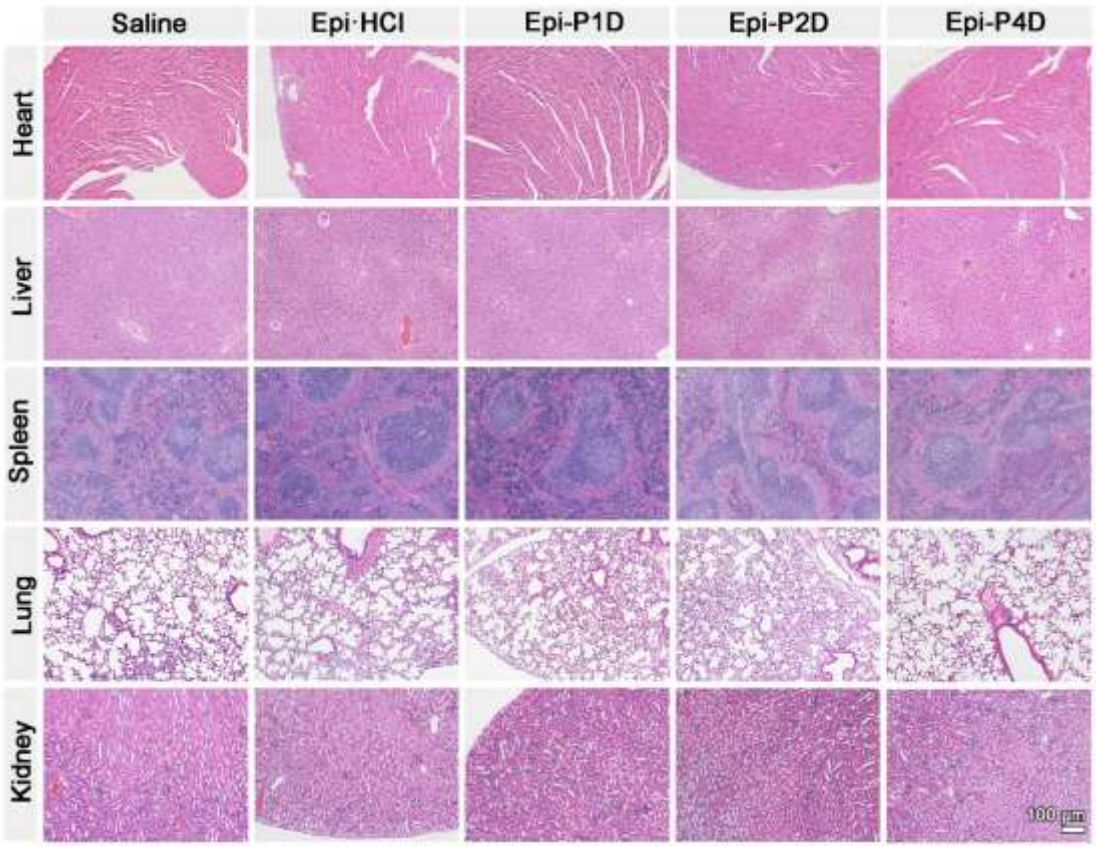

Figure S42 H&E staining images of major organs, including the heart, liver, spleen, lung, and kidney of the CT26 tumor-bearing mice after different treatments.

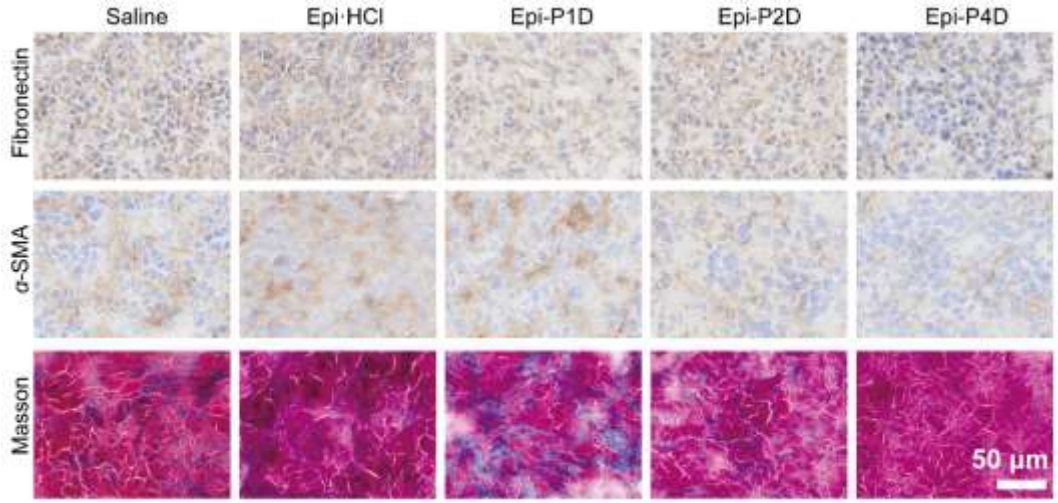

Figure S43 Immunohistochemical staining images of fibronectin (brown), α-SMA (brown), and collagen (masson staining, blue) in the 4T1 tumor tissue after a single intravenous injection of saline, Epi·HCl, or Epi-PD at an Epi dose of 8 mg/kg for 24 h.

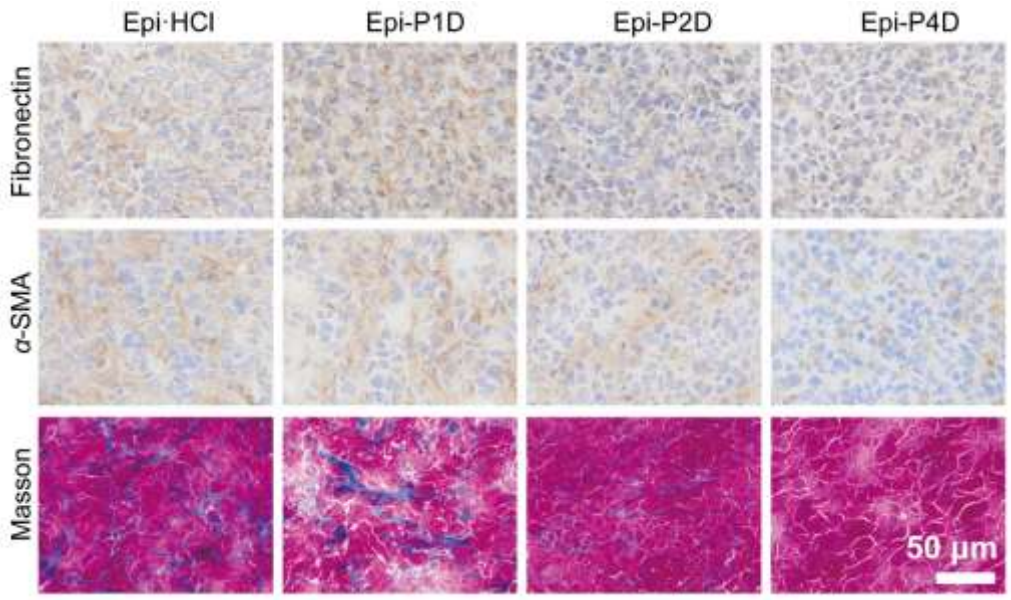

Figure S44 Immunohistochemical staining images of fibronectin (brown), α-SMA (brown), and collagen (masson staining, blue) in the 4T1 tumor tissue after a single intravenous injection of Epi·HCl or Epi-PD at an Epi dose of 8 mg/kg for 48 h.

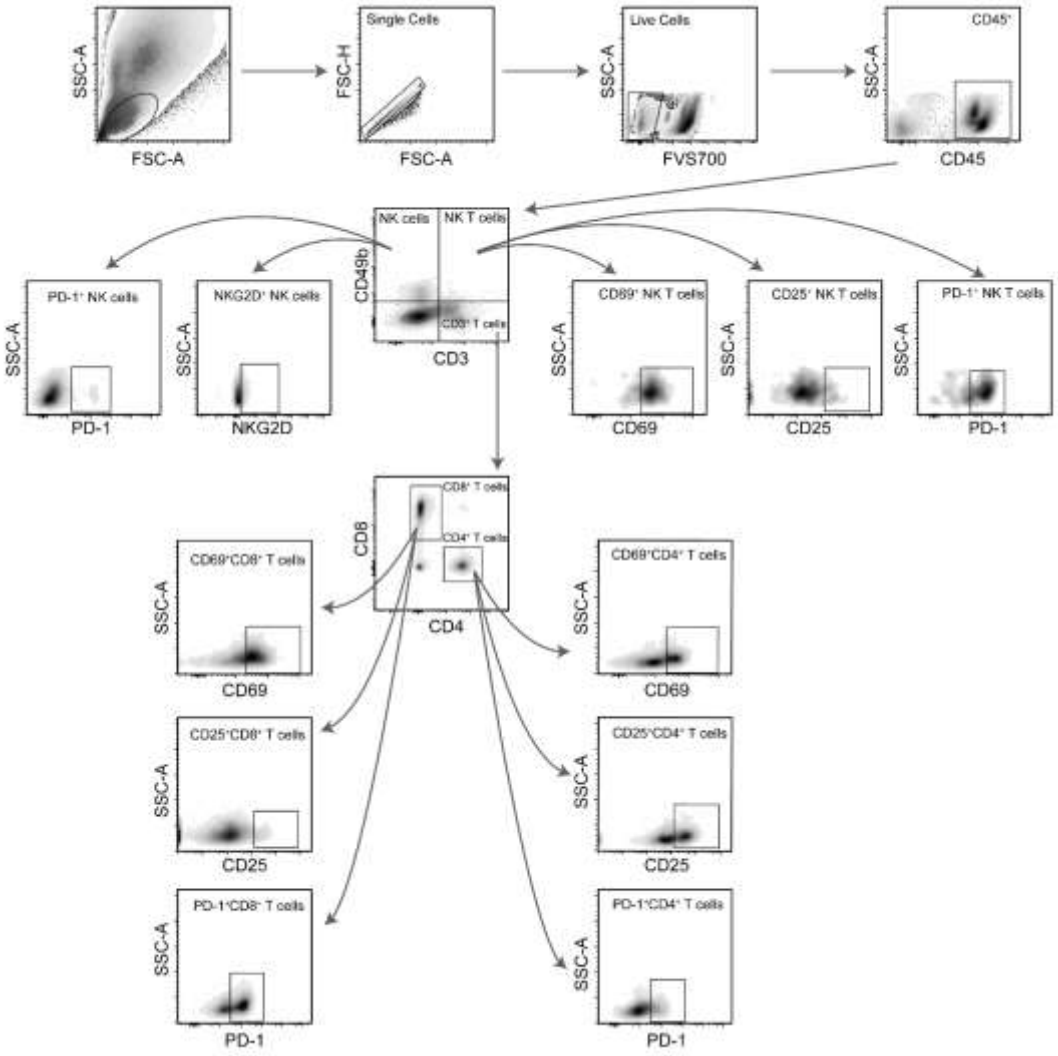

Figure S45 Gating strategies for the analysis of NK cells ($CD49b^+$ in $CD45^+CD3^-$ cells), NK T cells ($CD49b^+$ in $CD45^+CD3^+$ cells), $CD4^+$ T cells ($CD4^+$ in $CD45^+CD3^+$ cells), and $CD8^+$ T cells ($CD8^+$ in $CD45^+CD3^+$ cells) and their subpopulations, including activated ($NKG2D^+$ for NK cells and $CD69^+$ for T cells), hyperactivated ($CD25^+$ for T cells) and exhausted ($PD\text{-}1^+$ for all cells).

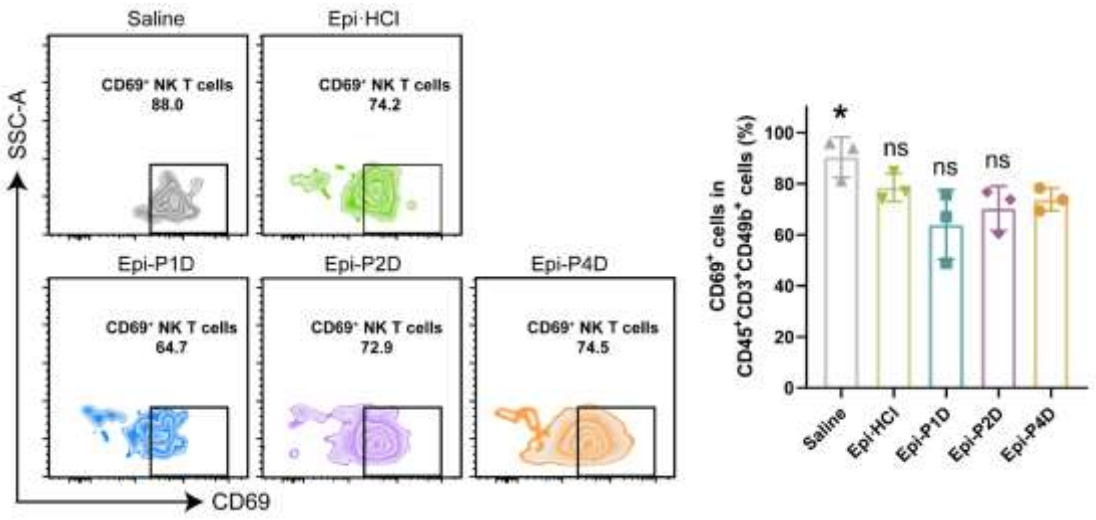

Figure S46 Flow cytometry diagrams (left) and percentages (right) of the activated NK T cells ($CD69^+$ in $CD45^+CD3^+CD49b^+$ cells) in CT26 tumor tissues after different treatments (Data are mean ± SD, n = 3). ns, not significant, and $^*P < 0.05$ compared with the group treated with Epi-P4D.

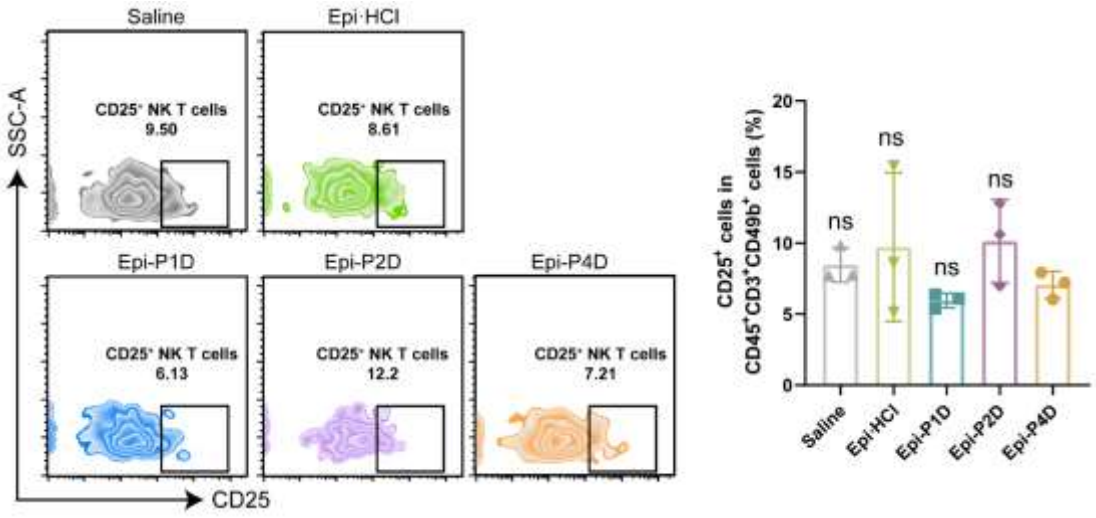

Figure S47 Flow cytometry diagrams (left) and percentages (right) of the hyperactivated NK T cells ($CD25^+$ in $CD45^+CD3^+CD49b^+$ cells) in CT26 tumor tissues after different treatments (Data are mean ± SD, n = 3). ns, not significant, compared with the group treated with Epi-P4D.

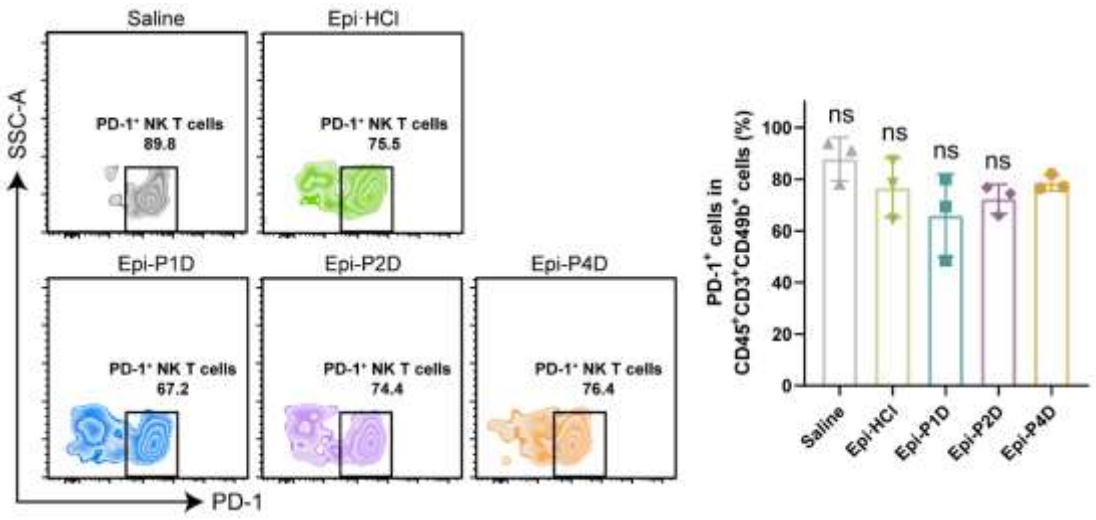

Figure S48 Flow cytometry diagrams (left) and percentages (right) of the exhausted NK T cells (PD-1$^+$ in CD45$^+$CD3$^+$CD49b$^+$ cells) in CT26 tumor tissues after different treatments (Data are mean ± SD, n = 3). ns, not significant, compared with the group treated with Epi-P4D.

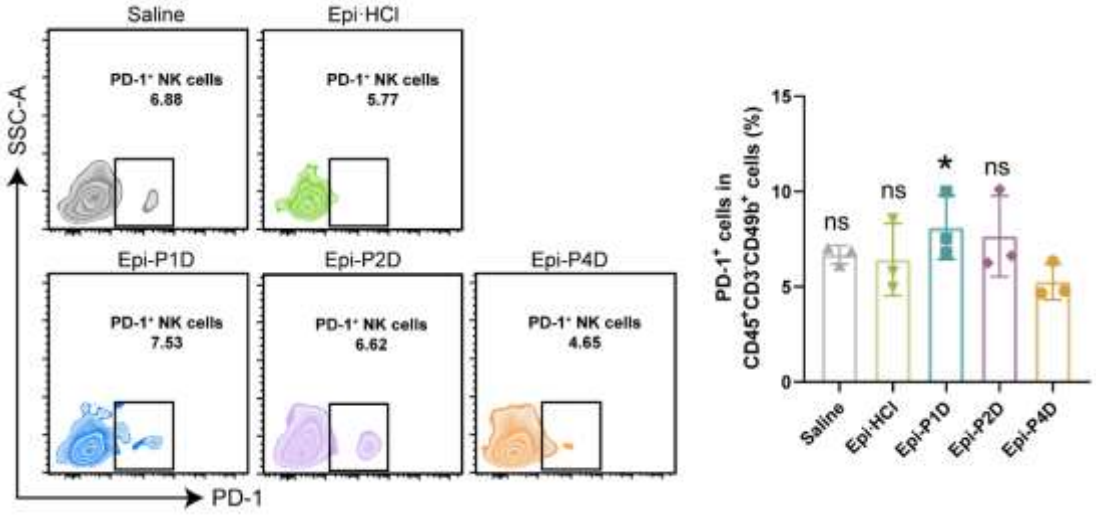

Figure S49 Flow cytometry diagrams (left) and percentages (right) of the exhausted NK cells (PD-1$^+$ in CD45$^+$CD3$^-$CD49b$^+$ cells) in CT26 tumor tissues after different treatments (Data are mean ± SD, n = 3). ns, not significant, and *P < 0.05 compared with the group treated with Epi-P4D.

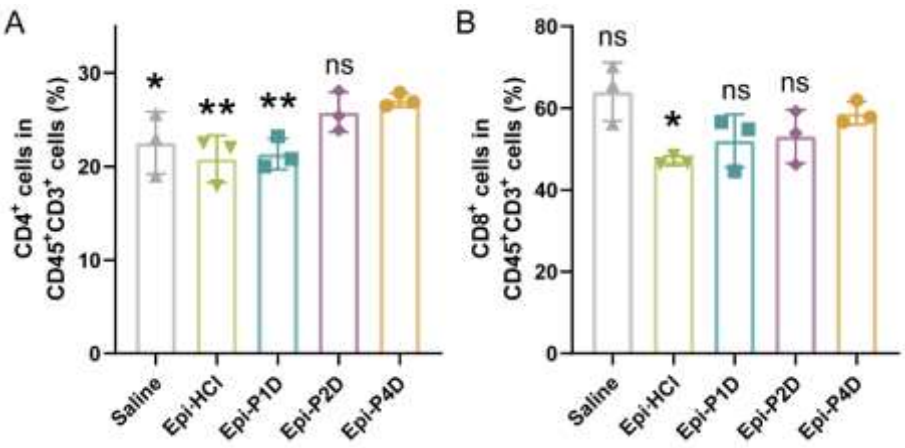

Figure S50 Percentages of (A) $CD4^+$ T cells ($CD4^+$ in $CD45^+CD3^+$ cells) and (B) $CD8^+$ T cells ($CD8^+$ in $CD45^+CD3^+$ cells) in CT26 tumor tissues after different treatments (Data are mean ± SD, $n = 3$). ns, not significant, $^*P < 0.05$, and $^{**}P < 0.01$ compared with the group treated with Epi-P4D.

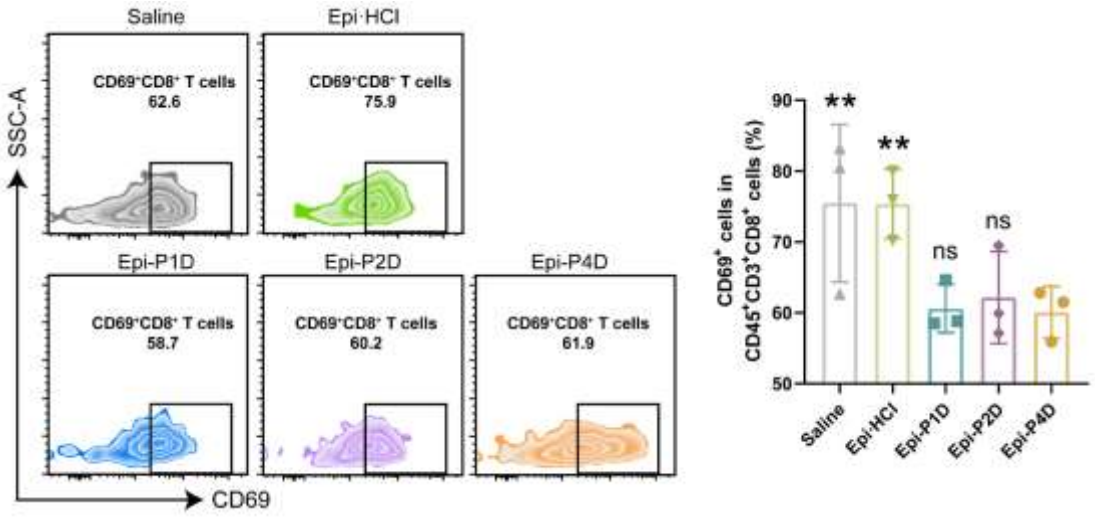

Figure S51 Flow cytometry diagrams (left) and percentages (right) of the activated $CD8^+$ T cells ($CD69^+$ in $CD45^+CD3^+CD8^+$ cells) in CT26 tumor tissues after different treatments (Data are mean ± SD, $n = 3$). ns, not significant, and $^{**}P < 0.01$ compared with the group treated with Epi-P4D.

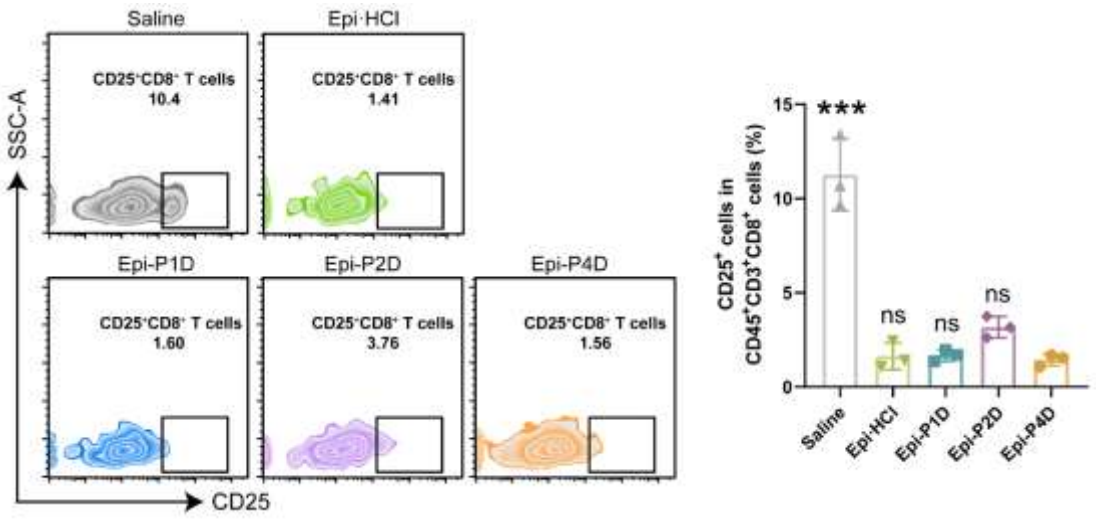

Figure S52 Flow cytometry diagrams (left) and percentages (right) of the hyperactivated $CD8^+$ T cells ($CD25^+$ in $CD45^+CD3^+CD8^+$ cells) in CT26 tumor tissues after different treatments (Data are mean ± SD, n = 3). ns, not significant, and ***P < 0.001 compared with the group treated with Epi-P4D.

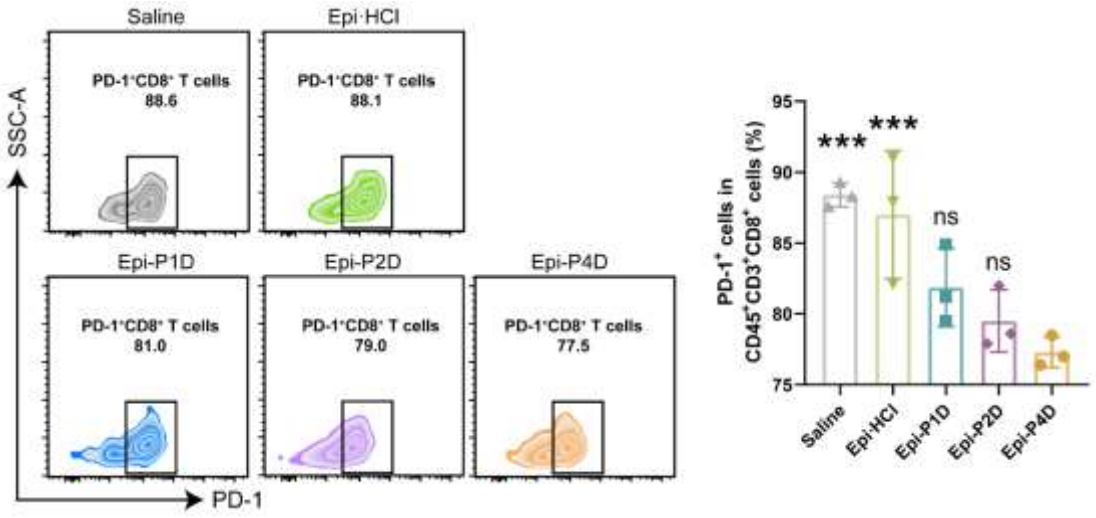

Figure S53 Flow cytometry diagrams (left) and percentages (right) of the exhausted $CD8^+$ T cells ($PD\text{-}1^+$ in $CD45^+CD3^+CD8^+$ cells) in CT26 tumor tissues after different treatments (Data are mean ± SD, n = 3). ns, not significant, and ***P < 0.001 compared with the group treated with Epi-P4D.

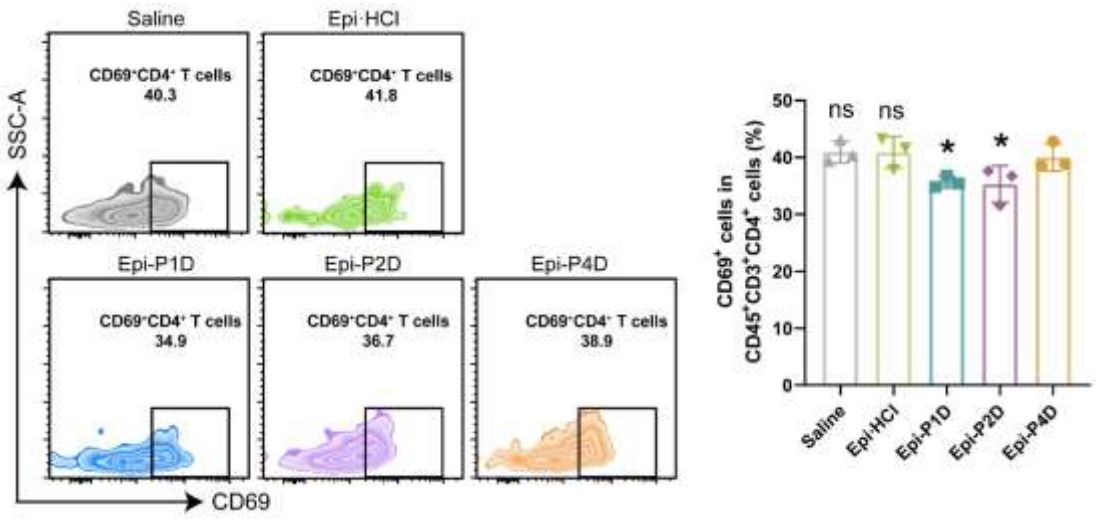

Figure S54 Flow cytometry diagrams (left) and percentages (right) of the activated $CD4^+$ T cells ($CD69^+$ in $CD45^+CD3^+CD4^+$ cells) in CT26 tumor tissues after different treatments (Data are mean ± SD, n = 3). ns, not significant, and $^*P < 0.05$ compared with the group treated with Epi-P4D.

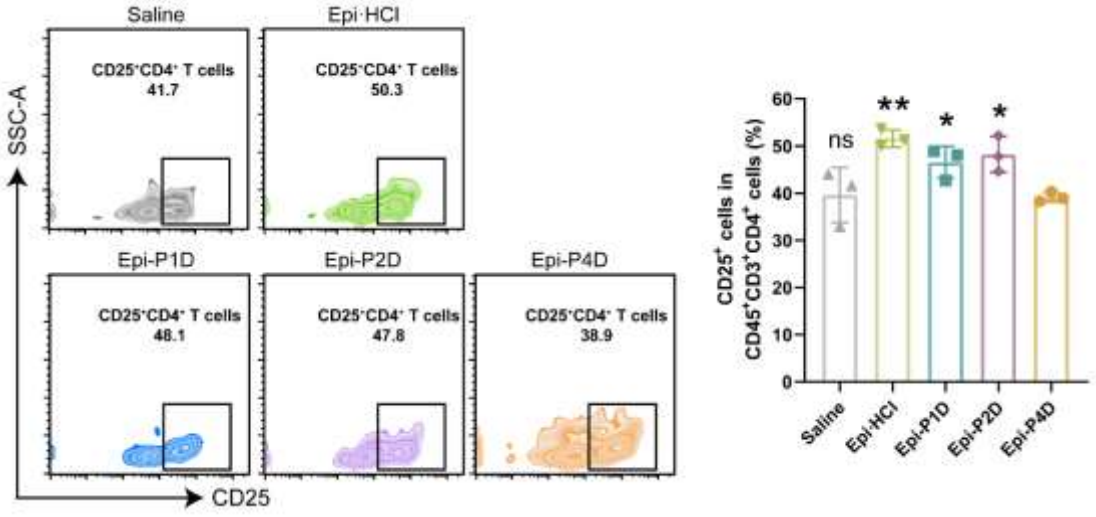

Figure S55 Flow cytometry diagrams (left) and percentages (right) of the hyperactivated $CD4^+$ T cells ($CD25^+$ in $CD45^+CD3^+CD4^+$ cells) in CT26 tumor tissues after different treatments (Data are mean ± SD, n = 3). ns, not significant, $^*P < 0.05$, and $^{**}P < 0.01$ compared with the group treated with Epi-P4D.

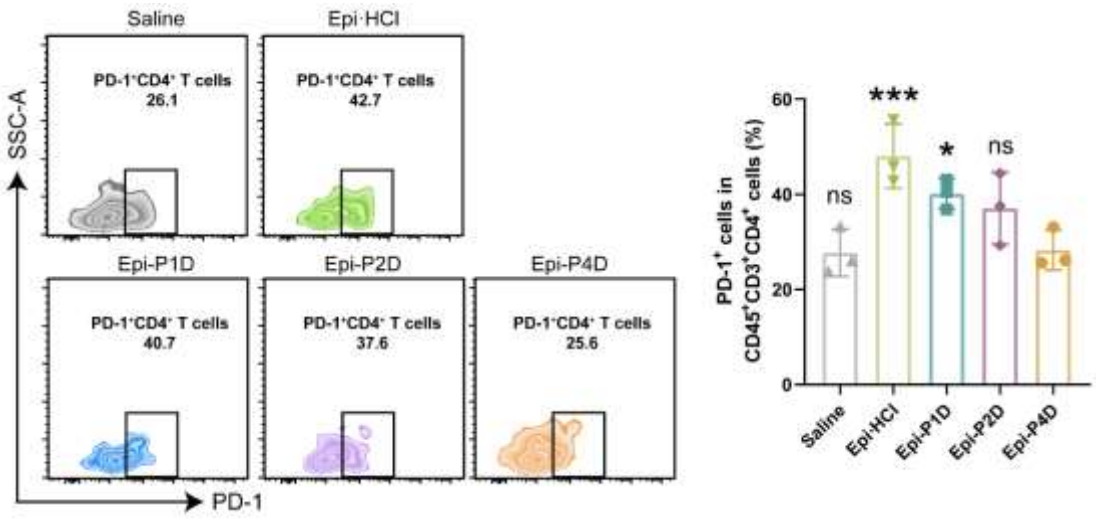

Figure S56 Flow cytometry diagrams (left) and percentages (right) of the exhausted $CD4^+$ T cells ($PD\text{-}1^+$ in $CD45^+CD3^+CD4^+$ cells) in CT26 tumor tissues after different treatments (Data are mean ± SD, n = 3). ns, not significant, *P < 0.05, and ***P < 0.001 compared with the group treated with Epi-P4D.

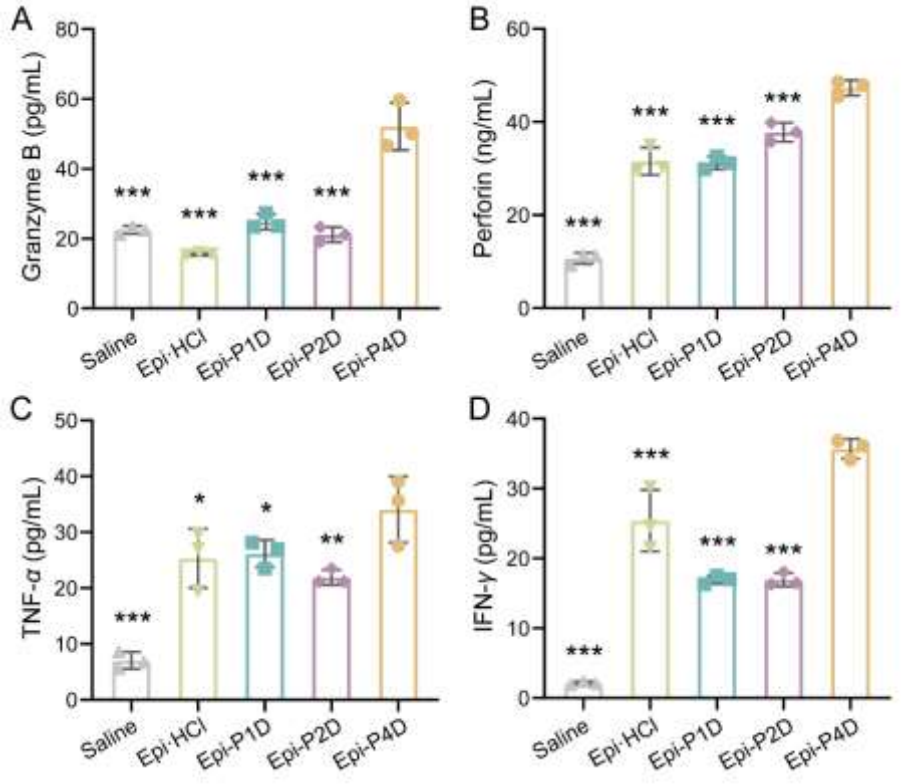

Figure S57 The cytokine level of (A) granzyme B, (B) perforin, (C) TNF-α, and (D) IFN-γ in the serum after different treatments (Data are mean ± SD, n = 3). *P < 0.05, **P < 0.01, and ***P < 0.001 compared with the group treated with Epi-P4D.

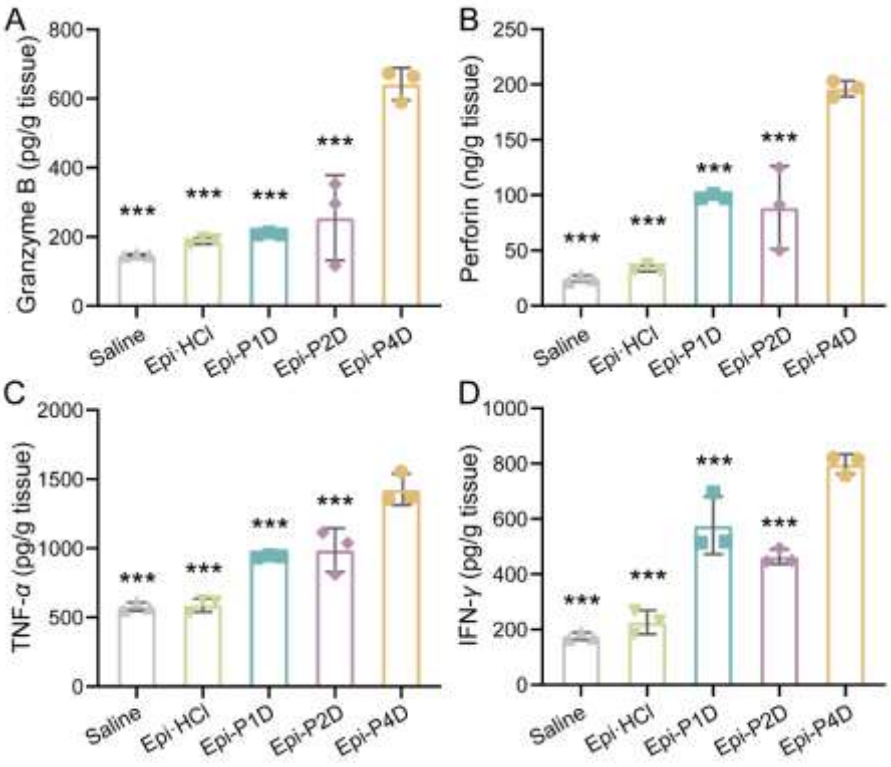

Figure S58 The cytokine level of (A) granzyme B, (B) perforin, (C) TNF-*α*, and (D) IFN-*γ* in CT26 tumor tissues after different treatments (Data are mean ± SD, $n = 3$). ***$P < 0.001$ compared with the group treated with Epi-P4D.

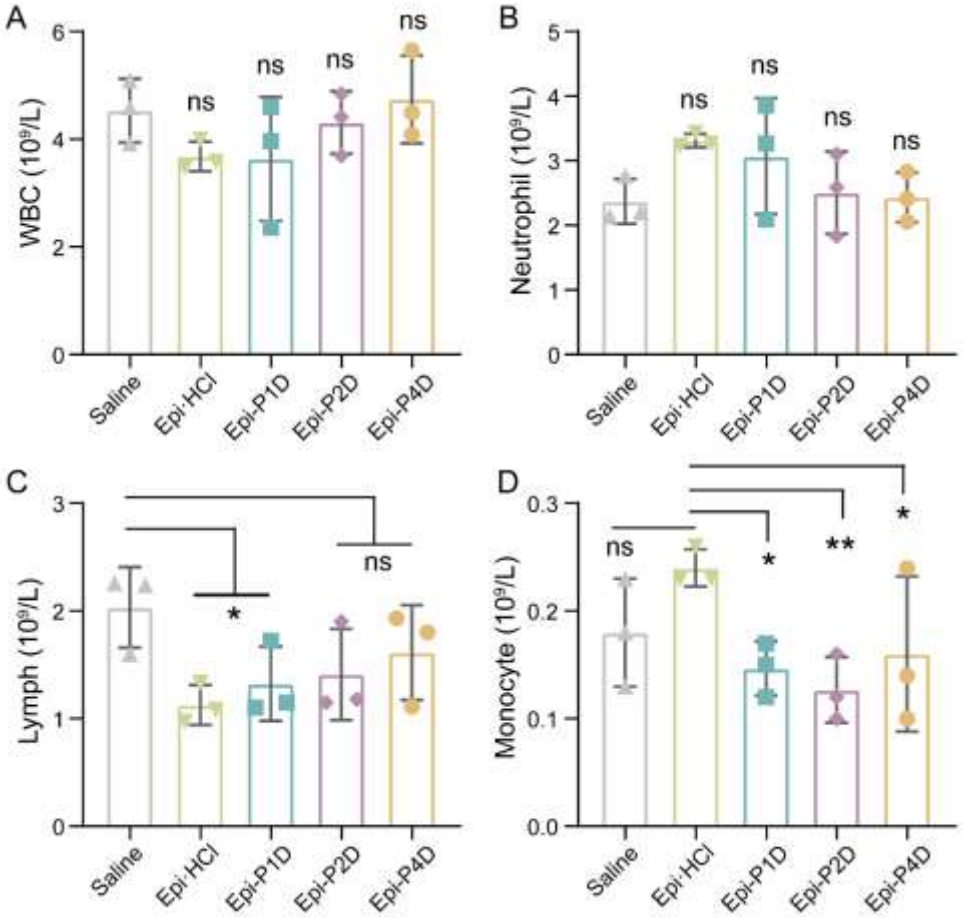

Figure S59 The number of (A) white blood cells (WBCs), (B) neutrophils, (C) lymphocytes, and (D) monocytes in the blood of the CT26 tumor-bearing mice after Epi·HCl, Epi-P1D, Epi-P2D, or Epi-P4D treatment (Data are mean ± SD, n = 3). The tumor-bearing mice injected with saline were used as a control. In (A)–(C), ns, not significant, and *P < 0.05 compared with the group treated with saline. In (D), ns, not significant, *P < 0.05 and **P < 0.01 compared with the group treated with Epi·HCl.

3. Supplementary tables

Table S1. The Epi content in Epi-PD

	Epi content (%)
Epi-P1D	27.61 ± 0.63
Epi-P2D	17.48 ± 0.70
Epi-P4D	6.29 ± 0.32

Table S2. Zeta potentials of Epi-PD

	Zeta Potential (mV)
Epi-P1D	–13.51 ± 0.94
Epi-P2D	–17.11 ± 1.05
Epi-P4D	–20.42 ± 1.02

Table S3. Pharmacokinetic parameters of Epi in the blood of the mice after a single administration of Epi·HCl, Epi-P1D, Epi-P2D and Epi-P4D at an Epi dosage of 5 mg/kg (n = 4)

	Unit	Epi·HCl	Epi-P1D	Epi-P2D	Epi-P4D
C_{max}	μg/mL	13.57	18.72	19.39	24.15
AUC	μg/mL*h	14.75	82.66	77.94	120.22
$t_{1/2}$	h	1.11	3.94	5.28	6.72

C_{max}, the maximal Epi concentration;

AUC, the area under the curve;

$t_{1/2}$, the half-life time.

4. References

1. Wu HY, Zhong D, Zhang ZJ, Li YC, Zhang X, Li YK, et al. Bioinspired artificial tobacco mosaic virus with combined oncolytic properties to completely destroy multidrug-resistant cancer. *Adv Mater* 2020;**32**:1904958.
2. Li YK, Wu YH, Fang ZX, Zhang YX, Ding HT, Ren L, et al. Dendritic nanomedicine with boronate bonds for augmented chemo-immunotherapy *via* synergistic modulation of tumor immune microenvironment. *Adv Mater* 2024;**36**:2307263.
3. Liu K, Dong XZ, Wang Y, Wu XP, Dai HL. Dopamine-modified chitosan hydrogel for spinal cord injury. *Carbohydr Polym* 2022;**298**:120047.
4. Zhong D, Xu XH, Li YK, Wu HY, Zhang ZJ, Yang J, et al. Entirely synthetic bacterial nanomimics for highly-effective tumor suppression and immune elicitation. *Nano Today* 2020;**35**:100950.